Coprecipitation nanoarchitectonics for the synthesis of magnetite: a review of mechanism and characterization

Ancuţa Roxana Trifoi[2] · **Ecaterina Matei**[2] · **Maria Râpă**[2] ·
Andrei-Constantin Berbecaru[2] · **Caşen Panaitescu**[1] · **Ionut Banu**[3] ·
Rami Doukeh[1]

Abstract

Magnetite nanoparticles have attracted interest of researchers from different science fields such as medicine, biology, physics, or chemistry due to their multifunctional properties including biocompatibility, superparamagnetism and low toxicity. Several methods have been developed to synthesize magnetic nanoparticles with controlled size, shape, and magnetic properties. Among them, coprecipitation is the most widely used because of several advantages such as high-yield production of nanoparticles, its simplicity, low-cost and its eco-friendly reaction conditions, but it also has low reproducibility. To achieve the magnetic nanoparticles with the desired properties, the investigation and control of reaction parameters are essential. In this article, the mechanism of coprecipitation reaction for magnetite nanoparticle synthesis and recent studies in reaction parameters controlling the particle properties will be reviewed. In addition, the most used methods for structural and magnetic characterization of magnetite and magnetite functionalized nanoparticles are presented and exemplified.

Keywords Magnetite · Nanoparticle · Coprecipitation · Structural characterization · Superparamagnetism

Introduction

During the recent decades, magnetite (Fe_3O_4) nanoparticles have been attracted interest in many domains due to their specific properties such as biocompatibility, low toxicity, strong magnetization, high durability, and low price [1]. These characteristics of magnetite nanoparticles have been widely used in environmental remediation [2–7], drug delivery [8, 9], magnetic resonance imaging (MRI) [10], as anti-wear and friction reducing additives in lubricating oil [11] catalysis [12–14], electronics [15], biosensors [16, 17] and many other applications. All mentioned
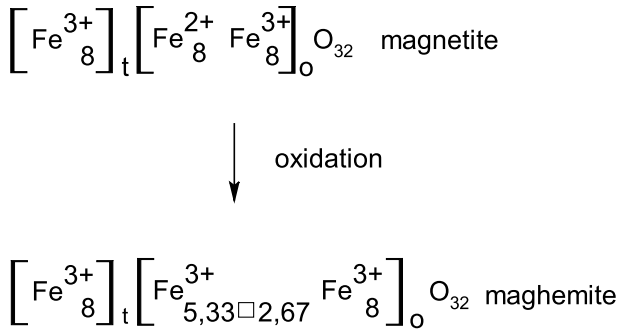
---

potential applications require specific properties of magnetite nanoparticles, so in order to obtain the necessary chemical composition, shape, size, surface properties and magnetic properties, diverse methodologies to synthesize and functionalize them have been developed. These methods include chemical coprecipitation [18], thermal decomposition [19], micro emulsion [20], sol–gel [21], hydrothermal method [22], electrochemical method [23], bacterial method [24], ultrasonic assisted reverse coprecipitation [25], other combined procedures [26], etc.

The coprecipitation method is the most widely used process for magnetite nanoparticles synthesis because of the high yield of nanoparticles that can be synthesized, its simplicity, low-cost and its eco-friendly reaction conditions [27–29], very important characteristics for industrial applications. Compared to some other techniques, the coprecipitation method also has some disadvantages, such as low repeatability, inappropriate size distribution of the particles and low crystallinity degree [30–32]. The concentration, molar ratio of the reactants, pH and temperature are some important factors for controlling the phase and size of nanoparticles and saturation magnetization [33]. To achieve the magnetic nanoparticles with the desired properties, the investigation and control of the mentioned parameters are essential.

Although the coprecipitation method is one of the most used techniques for the synthesis of magnetite nanoparticles, the number of integrative papers analyzing the process parameters that influence the yield and the properties of the particles is scarce. In this work, a comprehensive review focused on coprecipitation technique for synthesis of magnetite nanoparticles is presented. It highlights the synthesis parameters influencing the properties of the magnetite nanoparticles and provides a short guide to the young and senior researchers working in this domain to work with convenient process parameters and to properly characterize them. The pH of the solution and the precipitating agent, temperature, ion precursor and ionic strength, and stirring rate have been discussed, exemplified, and summarized. The mechanism of magnetite synthesis by coprecipitation method and the impurities formed during the process are also revised. Furthermore, a summary of magnetite and functionalized magnetite nanoparticles characterization methods is presented, with examples of each method and best practices, emphasizing their advantages and limitations (Scheme 1).

Crystal structure and properties of magnetite nanoparticles

Iron oxides exist in many forms in nature, among them magnetite (Fe_3O_4), maghemite (γ-Fe_2O_3) and hematite (α-Fe_2O_3) being most popular. Magnetite, known also as magnetic iron ore or ferrous ferrite [34] is the most useful iron oxide and has been employed in various fields of applications, exhibiting the strongest magnetism among the transition metal oxides [35]. According to Teja and Koh [34], magnetite has an inverse spinel structure with Fe(III) ions distributed randomly between octahedral and tetrahedral sites, and Fe(II) ions in octahedral sites. The inverse spinel cubic structure, as reported by Kozlenko et al. [36] is given in Fig. 1. Magnetite crystallizes with an inverse spinel cubic structure, with Fe^{3+} ions in the sites with tetrahedral oxygen coordination (A) and a mixture of Fe^{3+} and Fe^{2+} (equal proportion) in

$$\left[Fe^{3+}_{8}\right]_{t}\left[Fe^{2+}_{8}\ Fe^{3+}_{8}\right]_{o}O_{32}\quad\text{magnetite}$$

oxidation

$$\left[Fe^{3+}_{8}\right]_{t}\left[Fe^{3+}_{5,33}\square_{2,67}\ Fe^{3+}_{8}\right]_{o}O_{32}\quad\text{maghemite}$$

Scheme 1 Chemical representation of magnetite and maghemite structure [39, 40] Here t is tetrahedral site, o is octahedral site, and $\square$ is vacancy
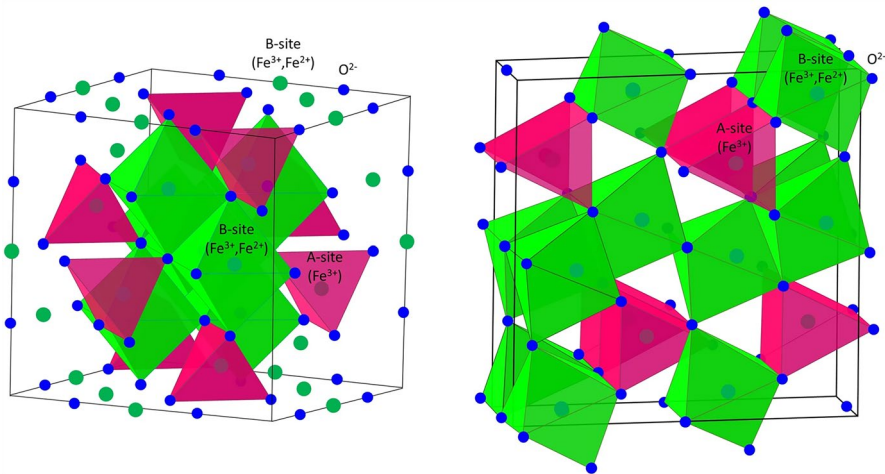

Fig. 1 The inverse spinel cubic (left) and post-spinel orthorhombic (right) crystal structure of magnetite. The **A** iron sites with tetrahedral (in the spinel structure) or prismatic (in the post-spinel structure) oxygen coordination and **B** iron sites with the octahedral oxygen coordination are shown—reproduced from [36]

the sites with octahedral oxygen coordination (B). The iron spins at the A and B sublattices arranges ferromagnetically below the Néel temperature [36]. As mentioned by Narang and Pubby [37] the spinel ferrites have 8 divalent metal cations (Fe^{2+} for magnetite) at 8 of the available 16B-sites and 16 trivalent ferric cations (Fe^{3+}) at 8 A-sites and the remaining 8B-sites as per formula $\left[Fe^{3+}\downarrow\right]_{A}\left[Fe^{2+}\uparrow\ Fe^{3+}\uparrow\right]_{B}O_{4}^{2-}$, where $\downarrow$ and $\uparrow$ are the opposite spin directions of A and B sites. In magnetite case, Fe^{3+} ions acts both as network formers and network modifiers.

In magnetite, the ferrimagnetic moment appears due to the unpaired spins of Fe^{2+} in octahedral coordination. Concerning the Fe^{3+} ions, they are coupled anti-ferromagnetically via the oxygen atom, resulting in a net zero magnetization in the Fe^{3+} sub lattice. Octahedrally coordinated Fe^{3+} and Fe^{2+} ions are coupled

ferromagnetically through a double exchange mechanism, with an electron whose spin is directed in the opposite direction of the others that can be exchanged between two octahedral coordination sites [38]. The physical properties of magnetite are presented in Table 1.

Maghemite is formed by oxidation of magnetite. Maghemite has a similar cubic structure to magnetite, a spinel-inverted type structure, and presents unit cells with a vacancy of 2.67 cationic iron atoms located in octahedral sites. The chemical representation of magnetite and maghemite may be indicated as follows [39, 40]:

Coprecipitation vs. other methods

Coprecipitation is the traditional method for producing Fe_3O_4 [41, 42] involving the combination of ferric and ferrous ions in extremely basic solutions in a 1:2 molar ratio. Surfactants like dextran or polyvinyl alcohol can be added to the reaction media, or the particles can be coated in a subsequent stage, to produce well-dispersed magnetic nanoparticles [3]. Surfactants protect colloidal dispersions by regulating particle size and stabilizing it. However, because of the large particle size distribution, secondary size selection techniques are needed. Even while aqueous synthesis approaches for the preparation of magnetite nanoparticles have improved over the past ten years, they is still one significant drawback, the difficulty to properly control particle size [43].

Table 1 The properties of magnetite [29, 145]

Properties	
Molecular formula	Fe_3O_4
Color	Black
Crystal structure	Cubic
Molecular structure	Inverse spinel
Cell dimension/Lattice parameters (nm)	a = 0.8396
Formula units, per unit cell, Z	8
Density (g/cm^3)	5.18
Mohs hardness	5.5
Type of magnetism	Ferrimagnetic (bulk) super-paramagnetic (nanoparticles)
Saturation magnetization, Ms (emu/g) at 300 K	92–100
Band gap energy (eV)	2.6
Curie temperature (K)	858
Standard free energy of formation, ΔG^0_f (kJ/mol)	− 1012.6
Melting point (°C)	1583–1597
Boiling point (°C)	2623

Thermal decomposition syntheses are currently viewed as the most popular way to obtain magnetic nanoparticles, and alternatives to other approaches. The production of the magnetic magnetite/maghemite phases, on the other hand, happens later owing to oxidation upon exposure to air oxygen, according to recent research [44]. This suggests that the thermal decomposition routes may begin with the formation of a non-magnetic Wüstite phase. Additionally, thorough research using high-resolution transmission electron microscopy points to the presence of flaws and polycrystalline particles, which could ultimately influence the magnetic and functional properties of the nanoparticles. Due to this aspect, post-synthesis thermal oxidative treatments have been used to enhance the magnetic characteristics of the nanoparticles. These treatments work well for small particles (15 nm), but when particle size increases (above 20 nm), these approaches lose their effectiveness or require extremely long (> 30 h) processing times [19].

Precipitation in microemulsion has been proved as a potential technique for producing magnetic nanoparticles with improved control over size and morphology. A microemulsion is a stable isotropic dispersion of two immiscible liquids that is stabilized by an interfacial coating of surface-active molecules. It consists of nanosized domains of one liquid in the other. The confinement effect created by the surfactant molecules restricts the growth, nucleation, and agglomeration of particles. In this process, tiny water droplets (referred to as "water pools") that are uniformly dispersed in an oil phase co-precipitate with surfactant molecules. The water-to-surfactant molar ratio thermodynamically determines the size of these "water pools," also known as reverse micelles, which serve as micro reactors for the synthesis of nanoparticles [20].

Hydrothermal synthesis is one of the most popular methods for creating magnetic nanoparticles. As opposed to conventional crystal-making synthesis, which involves high temperatures and pressures, this technique produces single-crystal nanoparticles by depending on the solubility of an aqueous solution (water). It is essentially a synthesis approach based on solution reactions. From room temperature to extremely high temperatures (130–250 °C), hydrothermal synthesis of magnetic nanoparticles can take place at a variety of temperatures. It is possible to use the various vapor pressures in the reaction, either in low-pressure or high-pressure conditions (0 and 3–4 MPa), to control the morphology of the materials to be synthesized, resulting in the material crystallizing in a sealed container and greatly improving the preferential growth of different planes of the MNPs. However, compared to other, more straightforward, less expensive synthesis processes, the high pressure and temperatures sacrifice the magnetic properties of the nanoparticles [45].

The wet-chemical approach's classic and widely utilized sol–gel synthesis process is mostly employed to fabricate nanometric size materials (usually metal oxides) [46, 47]. A colloidal solution typically acts as the foundation for an interconnected network of separated particles. A gel, a continuous three-dimensional network that encloses the colloidal liquid phase, and a sol phase, a stable dispersion of colloidal particles in a solvent, shape the system. In a colloidal gel, the network is created by the collection of colloidal particles. A sub-colloidal aggregate's deposition on the particles in a polymer gel creates a polymeric sub-structure for those particles.

Due to hydrophilic ligands on the surface of magnetic nanoparticles, which are used in the surface coating and for high control over size and shape, the sol–gel reaction has definite advantages over the prior wet-chemical or aqueous synthesis method, such as the simple dispersion in solvents. However, the low yield compared to other approaches, like coprecipitation, the expensive costs of the reagent precursors (i.e., alkoxides), and the difficulty obtaining magnetite structure limit the convenience of this technique [45].

Among the traditional techniques for producing magnetic nanoparticles, electrochemical synthesis is starting to be promising. One benefit of this approach is the ability to regulate particle size by altering the electrooxidation system's imposed current density (i) or potential (E) [48, 49]. Additionally, it is possible to prevent particle aggregation if the synthesis is carried out in the presence of a surfactant. Using this technique,Cabrera et al. [23] produced Fe_3O_4 nanoparticles between 20 and 30 nm in size. Using standard techniques, it is impossible to obtain this size. Co-precipitation, for instance, produces smaller particles in the 5–12 nm range, whereas hydrolysis or sol–gel techniques can produce larger particles, but they can never be larger than 20 nm, and most of the time, they are difficult to suspend in an aqueous colloidal solution.

This promotes the quest for a method of water-based synthesis where the particle size might be around 20 nm or greater, which has been suggested as being excellent for heating and separation processes [50]. The produced particles, on the other hand, would be hydrophilic because the electrochemical synthesis of Fe_3O_4 is carried out in aqueous solution; as a result, their surface might be easily altered by exchange reactions with biomolecules of interest.

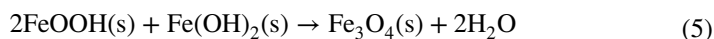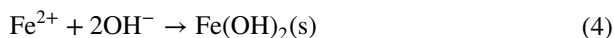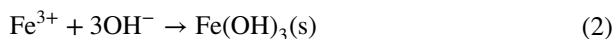## Magnetite nanoparticles synthesis by coprecipitation method

Mechanism

The synthesis of magnetite by coprecipitation is the most widely used method but the mechanism of particle formation is still not sufficiently explained, due to a lack of information on how intermediates are formed which may limit the reproducibility of the coprecipitation reaction. A comprehensive understanding of the mechanism is important not only for consistent synthesis, but also for adjusting particle properties for specific applications.

The overall chemical reaction of Fe_3O_4 precipitation is given in Eq. 1 [51]. The reaction is performed by using aqueous solutions of ferric (Fe^{3+}) and ferrous ions (Fe^{2+}) in an alkaline medium. The main steps of the mechanism consist of nucleation of iron oxide particles and post growth of the nuclei. The number of nucleus formed in the reaction and the size of the particles are strongly dependent on the experimental conditions, wherein the pH of the solution is considered to best control the nucleation and growth of the magnetite nanoparticles and can influence the magnetite properties, e.g., particle size and size distribution or saturation magnetization [52].

$$Fe^{2+} + 2Fe^{3+} + 8OH^- \rightarrow Fe_3O_4 + 4H_2O \tag{1}$$
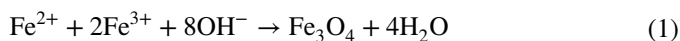
The possible reaction mechanism of iron oxide nanoparticles formation is shown in the following chemical reactions (Eqs. 2–5) [52]:

$$Fe^{3+} + 3OH^- \rightarrow Fe(OH)_3(s) \tag{2}$$

$$Fe(OH)_3(s) \rightarrow FeOOH(s) + H_2O \tag{3}$$

$$Fe^{2+} + 2OH^- \rightarrow Fe(OH)_2(s) \tag{4}$$

$$2FeOOH(s) + Fe(OH)_2(s) \rightarrow Fe_3O_4(s) + 2H_2O \tag{5}$$

Initially, the Fe^{3+} and Fe^{2+} hydroxides are precipitated very fast, followed by the ferric hydroxide decomposition to FeOOH. Then a solid state reaction between FeOOH (s) and $Fe(OH)_2$ (s) takes place with the formation of magnetite [52]. The most commonly noticed impurity compounds in magnetite synthesized by the coprecipitation method are maghemite, goethite and some hematite but absence or low oxygen can limit the transformation of magnetite to other phases [30]. A side reaction that takes place in the presence of oxygen is oxidation of Fe^{2+} and Fe^{3+}. To overcome this problem, two approaches have been used. In the first approach, the nitrogen (N_2) gas is bubbled into the reaction mixture or, other works presents the synthesis of magnetite nanoparticles under oxidizing environment (air atmosphere) by lowering the initial molar ratio (Fe^{3+}: Fe^{2+} < 2:1), so that after the oxidation of Fe^{2+} to Fe^{3+} the ratio approaches to 2:1.

The growth mechanism of iron oxide nanoparticles using Na_2CO_3 as a precipitating agent was studied by LaGrow et al. [53]. Na_2CO_3 was chosen as a precipitating base because of the slower growth kinetics than the kinetics when using stronger bases [54]. The experiments were carried out at 60 °C in a flow reactor and therefore the particle analysis was carried out in solution, during the synthesis, with the help of synchrotron X-Ray diffraction. At pH 12, two initial phases were formed: ferrihydrite phase, formed mainly of Fe^{3+} (poorly crystalline) and iron hydroxide carbonate, formed primarily of Fe^{2+} (crystalline) [53].

Using X-ray diffraction, electron microscopy, and Fourier-transform infrared spectroscopy (FTIR) Ahn et al. [55] showed that when the pH of the iron salt solution increased slowly and continuously, first nucleated was akageneite, which transformed to goethite, that had a topotactic transition to magnetite (the upper route in Fig. 2). An abrupt pH change results in different particle formation routes than slow base additions, showing the precipitation of ferrous hydroxide [$Fe(OH)_2$] and its transition to several intermediate phases including lepidocrocite (the under route in Fig. 2). Magnetite nanoparticles were formed within the coprecipitation process by the phase transformation of iron oxyhydroxides, instead of the direct reaction of Fe^{2+} and Fe^{3+} in the aqueous phase [55].

The "LaMer model" is often used to interpret the size distributions of the synthesized iron oxide nanoparticles. According to the LaMer model, a short instantaneous
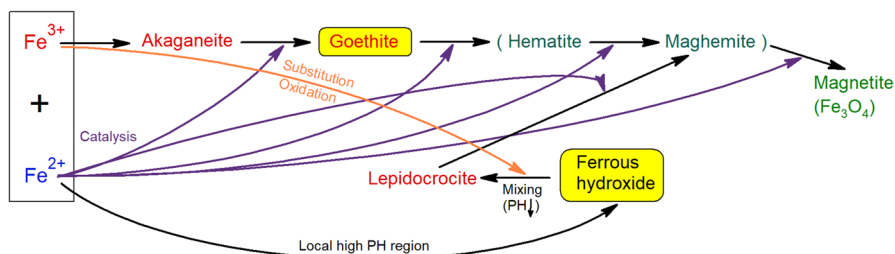
Fig. 2 Formation pathways of magnetite nanoparticles by coprecipitation method, influenced by the base addition speed, Reprinted with permission from Ref. [55], J. Phys. Chem. C. (2012), 116, Copyright © American Chemical Society

nucleation followed by slow controlled growth, without further nucleation, is the key to producing colloids with a narrow size distribution [56]. For iron oxide nanoparticles, the model is often cited as a diagrammatic drawing and description of the model is only associated with words. A further perspective on mechanism elucidation is the experimental evidence that the LaMer model fits the experimental nucleation kinetics data of iron oxide nanoparticles.

Operating parameters

The selectivity, morphology, and particle size of magnetite in the solution is quite sensitive and depends on operating parameters such as pH, reaction temperature, iron precursors and their concentration, optional presence of stabilizers/ligands, sequence of reagents etc. Table 2 summarizes the influence of several coprecipitation reaction parameters on different properties of magnetic particles. Hereinafter, a detailed description of each parameter is presented.

Effect of pH and precipitating agent

Magnetic iron nanoparticles can be synthesized by coprecipitation method, in alkaline conditions using different bases (NaOH, KOH, NH$_4$OH etc.). According to the thermodynamics of the reaction, complete precipitation of Fe$_3$O$_4$ should be expected at a pH between 8 and 14, with a stoichiometric ratio of 2:1 (Fe^{3+}/Fe^{2+}) in a non-oxidizing environment [57]. A strong alkaline medium (such as NaOH, KOH, or LiOH) can lead to formation of nonmagnetic iron components, so in order to avoid this, weak bases such as NH$_4$OH or Na$_2$CO$_3$ are recommended in many studies [58, 59]. Gnanaprakash et al. [58] studied the effect of initial pH of iron salt solutions (before adding the precipitating agent) on the formation of magnetite nanoparticles. The saturation magnetization values decreased from about 58 emu/g to about 17 emu/g as the initial pH increased from 4.7 to 6.7 at room temperature of 25 °C (reaction conditions: Fe^{2+}/Fe^{3+} molar ratio = 1:2; precipitating agent 25% of aqueous ammonia; final pH = 10; oleic acid coating), due to the formation of goethite which contributes to a drop in saturation magnetization of the magnetic particles. This occurs because of Fe^{2+} ions oxidation to the

Table 2 Influence of some coprecipitation reaction parameters on the properties of magnetite nanoparticles

Parameter	Property	Dependence	References
pH value (pH)	Iron oxide phase (ip)	Initial pH increases—formation of nonmagnetic impurities occurs	[58]
	Dimension (d)	pH increases—d decreases pH increases—d increases	[54, 58, 151, 152]
	Shape (s)	acicular, round square	[54]
	Magnetism (M_s)	Initial pH increases—M_s decreases	[58]
Precipitating base agent (OH⁻)	Iron oxide phase (ip)	Strong OH⁻ can cause formation of nonmagnetic iron components	[58, 59]
	Dimension (d)	Strong OH⁻—d increases; wide particle size distribution	[39, 52, 54]
Temperature (T)	Iron oxide phase (ip)	T decreases—magnetite content increases	[73]
	Dimension (d)	T increases—d increases little influence of T	[60–62, 68, 153, 154]
	Magnetism	T increases—M_s increases Non-proportional	[60, 153, 155]
Fe^{3+}/Fe^{2+} ratio (r)	Iron oxide phase	r decreases—magnetite content increases	[156]
	Dimension	r decreases -d increases	[154]
	Magnetism	r increases -M_s decreases	[68]
Iron concentration (C_{Fe})	Dimension	C_{Fe} increases -d increases	[68, 154]
	Magnetism	C_{Fe} increases -M_s increases	[68]
Stirring speed (v)	Dimension	v increases -d decrease v increases -d decreases	[71–73, 76, 157]
	Magnetism	-	

ferric state driving to an excess of Fe^{3+} ions in the system. Furthermore, if the iron precursors are first dissolved in an acidic aqueous medium, the individual precipitation of iron hydroxides is avoided.

Sodium carbonate may be a convenient precipitating base to study the mechanism of magnetite formation because the precipitation is progressive, and it is possible to record the reaction changes. Also, by reducing the abrupt pH variations, a narrow particle size distribution is obtained [54]. This was also observed by Peternele et al. [39], in the case of the size of magnetic nanoparticles obtained using weak bases as precipitating agent (e.g. NH_4OH) is more uniform than those obtained with strong bases (e.g., NaOH) [39]. The effect of pH on the properties of the magnetic nano-structured particles was studied by Blanco-Andujar et al. [54], at pH values between 6 and 10, room temperature, stoichiometric mixture of ferrous and ferric chloride salts and using sodium carbonate as a precipitating agent. The morphology, particle size and formed phases were investigated by powder XRD and TEM and are presented in Table 3. The obtained nanoparticles showed an increase in average particle size of about 10 nm per pH unit for the magnetite phase for pH values of 8, 9 and 10.

The nature of alkali, the slow or fast addition of alkaline solution and the final pH of the solution were studied to evaluate their influence on the particle size of the magnetite, by Mascolo et al. [52]. To investigate how the nature of precipitating agent affects the particle sizes, experiments were carried out using different amounts of NaOH, KOH or $(C_2H_5)_4NOH$ (TEAOH) alkaline solutions. Smaller magnetite particles were obtained using KOH and TEAOH compared to NaOH. The fast addition of the base enabled the formation of smaller magnetite nanoparticles in comparison to those of the corresponding magnetite obtained by slow addition of the base. This is related to the continuous nucleation against growth [52]. The authors also concluded that a stoichiometric ratio of Fe^{3+}/Fe^{2+} equal to 2:1 in solid phase is best achieved at room temperature, in a range of pH values, from 10.0 to 13.0. At higher temperatures (70–80 °C), the ratio between Fe^{3+}/Fe^{2+} is 2/1 at pH values between 9 and 12.

Table 3 Iron oxides nanoparticles and their characteristics, obtained by coprecipitation method at different pH values, using Na_2CO_3 as precipitating agent. Copyright with the permission of © The Royal Society of Chemistry 2012 [54]

pH	Particle size	Morphology	Phase
6	30 ± 4 nm long and 3.2 ± 0.4 nm wide	Homogeneous acicular shape	Goethite (a-FeOOH)
7	440 ± 65 nm 31 ± 1 nm and 4 ± 1 nm width	Nearly square nanoparticles Acicular nanoparticles	Siderite ($Fe(CO_3)$)-primary phase Goethite- secondary phase
8	6.9 ± 0.4 nm Forming aggregates of 50–70 nm	Nearly square nanoparticles Acicular particles	Magnetite-primary phase Goethite- secondary phase Siderite-tertiary phase
9	18 ± 3 nm Forming aggregates of 34 nm	Spheroidal nanoparticles	Magnetite
10	28 ± 5 nm without aggregates	Square nanoparticles Acicular particles	Magnetite-primary phase Goethite- secondary phase (low percentage)

Effect of temperature

In most cases the syntheses of magnetic nanoparticles were performed at 70–80 °C or higher temperature and the size of the magnetic nanoparticles increases with reaction temperature, but there also are some studies that indicate an inconsiderable temperature dependence of magnetic nanoparticles properties.

Niu and Zheng [60] analyzed the properties of Fe_3O_4 nanoparticles (size and magnetic properties) synthesized by coprecipitation, at temperatures from 60 °C to 90 °C and observed an increase of particle size with the reaction temperature. Fe_3O_4 nanoparticles (determined by SEM), with a narrow size distribution were obtained by coprecipitation method, at 1.5 h reaction time, a stirring speed of 200 rpm and using ammonia solution as a precipitating agent. The size of nanoparticles varied from 30 to 60 nm, in proportion to the increasing reaction temperatures. It can be seen that the particle size has almost doubled (e.g., presented in the article 31.26 nm for 60 °C and 58.06 for 90 °C). Although all the samples have typical superparamagnetic behavior, the saturation magnetization (M_s) also changes with temperature. The highest saturation magnetization was for the particles synthesized at 70 °C (58.9 emu/g), probably due to the better degree of crystallinity than the others [60] and the lowest M_s was 45.6 emu/g for a synthesis temperature of 60 °C. Petcharoen and Sirivat [61] successfully controlled the nanoparticle size to be in the range of 10–40 nm, by varying the reaction temperature and surface modification. Therein, the particle size of bare magnetite also increases with temperature. The same effect was observed for hexanoic acid coated magnetite, but not for the oleic acid coated magnetite, where the particle size decrease with increasing temperature, probably due to steric hindrance of acid molecule [61].

The influence of temperature on magnetite nanoparticle band gap, size and morphology has been studied by Saragi et al. [62] from room temperature to 80 °C, at pH = 10. They obtained spherical nanoparticles and using TEM and Particle Size Analyzer observed that the average size of Fe_3O_4 nanoparticles has an irrelevant increase with temperature. They assigned it to the acceleration of chemical reaction between iron ions. The average particle size calculated from TEM measurement was 10.14 nm, 10.32 nm, 10.95 nm and 11.66 nm for synthesis temperature of 25 °C, 40 °C, 60 °C, and 80 °C. Even if an increase in particle size with temperature has been observed, it is not very significant. Comparable results have been obtained by Meng et al. [63], who investigated the temperature effect, among other parameters (pH, iron salts ratio and concentration, crystallization temperature) on particle size and saturation magnetization. No more than 2 nm, but, usually, a sub nanometer variation of particle size was observed in 40–70 °C temperature range. Also, the saturation magnetization was insignificantly affected by temperature, with a variation of 3 emu/g, in the same pH medium.

At high temperatures larger particles can be produced because at elevated temperatures the growth of nucleus is easier to happen, and the nucleation rate is slow down [64].

Effect of iron precursors and Fe3 + /Fe2 + ratio

Recent reports reveal that the kind of precursors influence the mean size, shape and magnetic properties of the magnetic nanoparticles synthesized by the coprecipitation method. The most used anions of iron salts consist of chloride, sulfate, and nitrate. The growth of oxide nanoparticles in aqueous solution can be controlled by controlling the ionic strength of the reaction solution [65]. So, by changing the iron salt, the ion strength of the solution changes.

Yazdani and Seddigh [66] explained the influence of precursor's anions on nanoparticle size based on ionic strength (I) and the double layer theory and it was attributed to the size of precursor anions. They used various iron salts, Fe^{2+}–$FeCl_2 \cdot 4H_2O$, $FeSO_4 \cdot 7H_2O$ and Fe^{3+}–$FeCl_3 \cdot 6H_2O$, $Fe_2(SO_4)_3$ and $Fe(NO_3)_3 \cdot 9H_2O$ precursors in varied combination, to obtain magnetite, using a NaOH solution, at 25 °C and under a nitrogen atmosphere. The increase in ionic strength results in reducing the size of the magnetic nanoparticles. For the solutions with the same ionic strength but different mean size of the particles the behavior was explained by the double layer theory. As the anion size of the precursor salt increases, the synthesized nanoparticles mean size decreases (Fig. 3).

Iwasaki et al. [67] studied the influence of iron precursors and coexisting anions in the formation process of Fe_3O_4 nanoparticles (at room temperature, sodium hydroxide- as precipitating agent, pH > 12, and argon atmosphere). They used in their experiments $FeCl_3 \cdot 6H_2O$ as Fe^{3+} ion source and $FeSO_4 \cdot 7H_2O$, $FeCl_2 \cdot 4H_2O$ or $Fe(C_3H_5O_3)_2 \cdot 3H_2O$ as Fe^{2+} ion source. The role of coexisting anions was investigated by adding sodium sulphate (SO_4^{2-} source), sodium chloride (Cl^- source) or sodium lactate ($C_3H_5O_3^-$ source), in water before the iron salts were dissolved. It was found that the presence of SO_4^{2-} coexisting ion has the effect of increasing the particle size. Contrarily, chloride and lactate contributed to size reduction of the Fe_3O_4. Table 4 presents the average crystallite size of magnetite nanoparticles obtained from XRD analysis [67]. Furthermore, when $FeSO_4$ was used as Fe^{2+} sources, goethite particles were also observed in the final product.
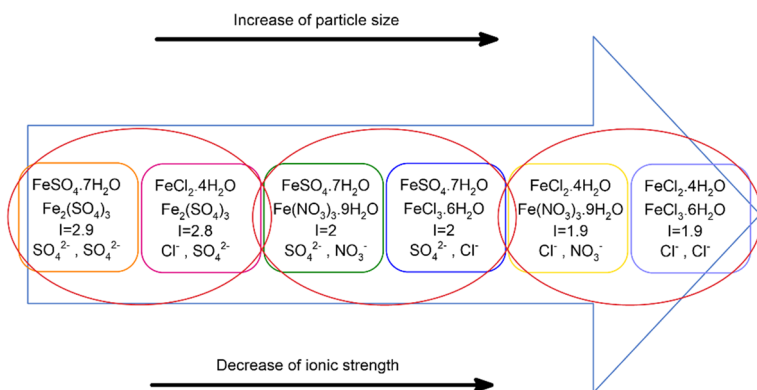

Fig. 3 The variation of magnetite nanoparticles size with ionic size and strength of the iron precursors, Reprinted with permission from Ref. [66], Mater. Chem. Phys. (2016), 184 © Copyright Elsevier

Table 4 The dimensional properties of the magnetite nanoparticles synthesized by Iwasaki et al. [67]

Ferrous ions source	Coexisting anions	Average crystallite size (nm)—from XRD analysis
$FeSO_4 \cdot 7H_2O$	None	–
$FeCl_2 \cdot 4H_2O$	None	10.9
$Fe(C_3H_5O_3)_2 \cdot 3H_2O$	None	4.9
$FeSO_4 \cdot 7H_2O$	Cl^-	11.4
$FeSO_4 \cdot 7H_2O$	$(C_3H_5O_3)^-$	9.7
$FeCl_2 \cdot 4H_2O$	SO_4^{2-}	7.4

Not only the type of iron precursor is important for acute control of the properties of magnetic nanoparticles, but also the ratio of Fe^{3+}/Fe^{2+} and the concentration of iron salts. Among other variables, Roth et al. [68] have explored the impact of Fe^{3+}/Fe^{2+} ratio and iron salts concentration in magnetization and in size of magnetic nanoparticles. They found that by modifying Fe^{3+}/Fe^{2+} the saturation magnetization (M_s) may be improved. The M_S increased from 62 to 82 A m^2 /kg by reducing the Fe^{3+}/Fe^{2+} molar ratio from 3 to 1.5 [68]. A similar influence of Fe^{3+}/Fe^{2+} ratio on M_S was reported earlier in literature [69, 70].

Effect of stirring rate

The precipitation reactions are very fast, and the effect of mixing is significant down to slow mixing speed. This phenomenon is more prominent at fast mixing conditions and will depend on the flow regime in the reactor. Only a few studies designed the influence of stirring rate on the particle size and distributions of the magnetite nanoparticles synthesized by the coprecipitation method. Thus, Valenzuela et al. [71] found that a stirring rate of 10,000 rpm is suitable to obtain magnetite nanoparticles with a mean diameter of about 10 nm. As expected, decreasing the stirring velocity led to larger particle size and a wider size distribution. An interesting observation is related to a higher stirring rate (25,000 rpm) leading to an increase in the solutions' core temperature during synthesis, that promotes the partial thermal transformation of magnetite to goethite [71]. Fadli et al. [72] synthesized magnetite crystallites of 10–12 nm, by coprecipitation method (Fe^{3+}/Fe^{2+} 2:1, 40–80 °C, pH 10 using ammonia solution as precipitating agent) at a stirring speed between 300 and 500 rpm. The higher the stirring speed was (500 rpm), the smallest magnetite crystallites were obtained (10 nm), the agglomeration of the particles became more uniform and the crystallinity of the magnetite phase increased. Other authors observed a similar effect too [73–75]. A higher stirring rate produces a faster seeding and thus, more seeds with smaller particles are formed compared to slower stirring rates [73]. The magnetite content in the iron oxide nanoparticles was only slightly affected by the stirring rate [73]. In another research study, magnetite nanoparticles with crystallite size ranging from 22 to 25 nm were reported in the case of using stirring rates between 500 and 900 rpm. Contrary to the previous studies, from

600 to 800 rpm the crystallite size was about 22 nm and for a higher stirring rate (900 rpm) the particle size increased to 25 nm [76].

An explanation for producing small-sized particles at high stirring speed to is that the sample obtains transport energy in the form of kinetic energy that can reduce the molecular weight of Fe_3O_4 and break the agglomeration so that the particle becomes small fragments [76]. As mentioned by Rahmawati et al. [76], due to the strong magnetic force, the Fe_3O_4 molecules can recombine to form a large particle.

Magnetite nanoparticles stabilization

Magnetic nanoparticles are very sensitive to oxidation and agglomeration, so important issues of magnetic nanoparticle are their protection against accumulation, chemical reactivity and degradation, because a change of the properties may affect and limit the use of magnetic nanoparticles [77]. When they are in dispersions medium, there are several possibilities to stabilize the magnetic nanoparticles: electrostatic, steric, or combined methods. Electrostatic stabilization consists in the addition of charged functionalized molecules to the particle surface or the choice of the solvent used in particle suspension. Electrostatic repulsion can be controlled through knowledge of the diffusion potential, instead steric forces are more difficult to anticipate and quantify [78].

Zeta potential (ζ) determination is very useful for determining the dispersion stability of nanoparticles in different media. In general, colloids with values for the ζ-potential in the range of 20–30 mV or higher are considered stable. When the potential is small, attractive forces may exceed this repulsion and the dispersion may break and flocculate. Highly positively or negatively charged particles tend to repel each other, thus forming stable colloidal solutions which show only minor trends to agglomerate. So, dispersions with high zeta potential (negative or positive) are electrically stabilized, while those with low zeta potentials tend to aggregate [79].

Xiong et al. [80] prepared stable (trimethoxysilyl)propylmethacrylate (MPS) chemically modified magnetite particles for over three months at room temperature. The authors measured the zeta potential the chemically modified magnetite particles in aqueous media, at different pH values, using a Malvern Zetasizer Nano ZS. The zeta potentials were higher in neutral and alkaline conditions than that in acidic medium, indicating a high stability of the particles in neutral and alkaline condition. The explanation to this behavior is related to the extended polymer chains and high electrostatic repulsions on the surface of the nanoparticles.

The stability of the coated magnetite nanoparticles is recommended to be tested in a dispersing media like the application environment of the nanoparticles. For example, if magnetic nanoparticles are used in medicine, the dispersing medium for zeta potential measurements should be close to that of biological environment and the biological fluid. Due to the interaction with the biological media, magnetite nanoparticles tend to destabilize and undergo to aggregation processes, leading to the significant increase in their hydrodynamic size, as well as changes in nanoparticles surface properties.Yu

et al. [81]tested the stability of tetramethylammonium hydroxide coated iron oxide nanoparticles (T-SPIONs) and citrate coated iron oxide nanoparticles (C-SPIONs) in water and three different biological media of PBS (phosphate buffered saline), RPMI (Roswell Park Memorial Institute Medium) and DMEM (Dulbecco's Modified Eagle's Medium). The stability was tested in terms of hydrodynamic diameter as a function of time, and zeta potential. Both SPIONs show good stability in water since the hydrodynamic diameter did not change up to 3 months. C-SPIONs showed robust stability in biological media of PBS and RPMI and destabilized in DMEM, while T-SPIONs were found to aggregate rapidly and in all tested biological media. The authors succeed to stabilize the T-SPIONs and C-SPIONs by adding BSA (bovine serum albumin) on their surface, which significantly enhanced their stability, with no aggregation phenomenon detected in 24 h.

To avoid oxidation, protect and stabilize the magnetite core, a wide range of coating agents can be employed to coat the magnetic particles: natural and synthetic polymers, silica, carboxyl group, noble metals, metal oxides and sulfides and so on. Furthermore, they can also increase wetting properties and binding flexibility for various applications. Coating Fe_3O_4 nanoparticles with silica (SiO_2) may prevent or reduce the agglomeration of the particles, and protect them from dissolution in acidic solution, because SiO_2 is chemically stable in acidic solution. Furthermore, silica has tunable properties and further functionalization can be easily achieved and it has a good biocompatibility and hydrophilicity, which are indispensable for biomedical applications [82]. There are two methods for coating Fe_3O_4 with silica, by acidic hydrolysis of silicate in aqueous solutions and the modified Stöber process. The silica shell thickness can be controlled by varying the experimental parameters: the reaction time, the ratio of TEOS/Fe_3O_4 and the concentration of Fe_3O_4 nanoparticles [83]. Karimi Pasandideh et al. [84]have coated Fe_3O_4 particles with SiO_2 to form core–shell particles that have been successfully applied in humic acid removal from water resources, in acidic conditions. Silica coated Fe_3O_4 particles have also been regenerated and reused several times. The carbon coating also provides an efficient oxidation protection and prevents corrosion of iron oxide [85].Besides stability over the entire pH range, the carbon coating also enhance the biocompatibility and dispersity of the particles. Noble metals such as gold and silver facilitate further functionalization and are also known to improve stability and compatibility [86]. The surface of the iron oxide can be coated with various natural polymers (e.g. chitosan, gelatine, dextran) or synthetic polymers (such as polylactic acid (PLA), polyethylene glycol (PEG), polyvinyl alcohol (PVA)) avoiding aggregation and improving chemical and thermal stability, hydrophilicity and biocompatibility [87–89].

Castelló et al. [90] have synthesized alginate and chitosan coated magnetic nanoparticles and tested their stability by monitoring their hydrodynamic diameters as a function of time. After a period of six months the hydrodynamic diameter did not change and no flocculation or settling of the particles was observed. In biological medium, alginate magnetic nanoparticles were stable for more than 9 days, while chitosan magnetic nanoparticles were stable for only 2 days.

Magnetite nanoparticles characterization

The characterization of any synthesized material is necessary to understand the scientific reason of its properties. A great review dealing with practices for characterization of magnetic nanoparticles for biomedical applications was written by Sandleret al. [91] who offered a simple explanation and background for preferred practices in the characterization methods and technologies associated with the magnetic nanoparticle field. The most common analytical techniques for the characterization of magnetic nanoparticles, but not limited to, with the advantages and restrictions collected from the literature, are summarized in Table 5.

Fourier transform infrared spectroscopy (FTIR) is a technique based on the measurement of the absorption of electromagnetic radiation with wavelengths within the mid-infrared region (4000–400 cm^{-1}).

FTIR analysis is an excellent technique to identify the functionalization of magnetite, but it can also be a useful technique to differentiate between different iron oxides. The absorption band at a high wavenumber region is due to OH stretching, and at lower wavenumber as a result of Fe–O lattice vibration. Namduri and Nasrazadani [92] established a quantitative analysis of iron oxides using FTIR. Binary mixtures of iron oxides were prepared with known compositions containing pure commercial magnetite, maghemite and hematite for calibration purposes. The authors selected the bands at 570 cm^{-1} (for magnetite), 540 cm^{-1} (for hematite) and 630 cm^{-1} (for maghemite) to set the calibration curve for known amounts of iron oxide. Table 6 summarizes FTIR absorption bands for different iron oxides, selected from the literature.

The presence of silica layer on the surface of magnetite was demonstrated using FTIR characterization by the vibration bands of Si–O bonds and silanol groups at wavenumbers around 800 and 1000–1100 cm^{-1}, bands that increased with silica loading. These bands were shifted from original, to smaller wavenumbers, indicating the interaction of siloxane with hydroxyl functionality of the magnetite nanoparticles, forming bonds of the type of Si–OH–Fe. Examples of the FTIR spectra of functionalized magnetite nanoparticles with different amounts of silica are shown in Fig. 4 [93]

Another category of widely used materials for magnetite functionalization are the polymers and the monomers because they can increase the stability of the nanoparticles and protect them in vitro and in vivo. The most used polymers or monomers for magnetite nanoparticles are polyethylene glycol (PEG) [94], glucose, dextran [95], chitosan [96], alginate [97], polyvinyl alcohol [98]. Sathyanarayanan and Raina [99] investigated the coating of magnetite surface with polymers like PEG and chitosan. Using FTIR, they demonstrated the absorption of PEG and chitosan on magnetite nanoparticles through absorption bands of C–H methyl stretch (2956 cm^{-1}), amide stretch (1641 cm^{-1} and 1371 cm^{-1}), C–C and C–O asymmetric and symmetric stretch (1087 cm^{-1}, 1041 cm^{-1}). The electrostatic interaction between the negatively charged obtained magnetite and positively charged chitosan (due to the amine groups) gave a minor shift of the peaks compared to the pure material.

Table 5 Selective analytical techniques for the characterization of magnetite and functionalized magnetite nanoparticles

Method	Physicochemical properties/use	Advantages	Restrictions/drawbacks
FTIR (Fourier transform Infrared spectroscopy)	Surface properties such as structure and conformation	Universal technique Sensitive, fast and easy	Aqueous solutions are very difficult to analyze Complex mixtures generate complex spectra
XRD X-ray diffraction analysis	For crystalline materials, shape, size, and structure determination	Nondestructive technique Rapid and simple analysis Can analyze mixed polymorphs	Sensitive to sample preparation techniques X-ray hazard Expensive
SEM Scanning electron microscopy	Morphology, size and size distribution	Relatively quick and simple sample preparation and image acquisition	Expensive Sample limitation Sample preparation can result in artefacts
TEM Transmission electron microscopy	Shape heterogeneity Size and size distribution Particle agglomeration	Powerful magnification and resolution Wide range of application Images are high quality and detailed	Difficulty in quantifying a large number of particles or misleading images due to orientation effects Laborious sample preparation
TGA Thermal gravimetric analysis	Mass and composition of the stabilizers	Simple and direct technique without the need of sample preparation	Need to have a few milligrams of the sample
DLS Dynamic light scattering	Size distribution based on hydrodynamic diameter Nanoparticles and colloids with low polydispersity	Measuring time for DLS is short and it is almost all automated Process is less labor intensive, and an extensive experience is not required for routine measurement Is extremely sensitive accurate size analysis of fine nanoparticles	Limited to dilute solutions sensitive to rare coarse particles (dust, agglomerates, contaminants)
XPS X-ray photoelectron spectroscopy	Surface chemical analysis	Non-destructive analysis without damaging the samples	Sample preparation (dry solid form, without contamination) Data analysis

Table 6 Infrared bands of different iron oxides and hydroxides

Iron oxide/hydroxide	Wavenumber (cm^{-1})	References
Magnetite (Fe$_3$O$_4$)	Broad bands at 570–590 and 360–400	[158–160]
Maghemite (γ-Fe$_2$O$_3$)	700, 630–660, 620, 430 range (Fe–O range)	[161, 162]
Hematite (α-Fe$_2$O$_3$)	540, 470 and 352	[163, 164]
Goethite (α-FeOOH)	1124, 890 and 795–810 cm^{-1} for OH stretch, 635	[164] [159, 163, 165]
Lepidocrocite (γ-FeOOH)	1020 cm^{-1} (in plane vibration) and 750 cm^{-1} (out of plane vibration), 620	[159, 166]
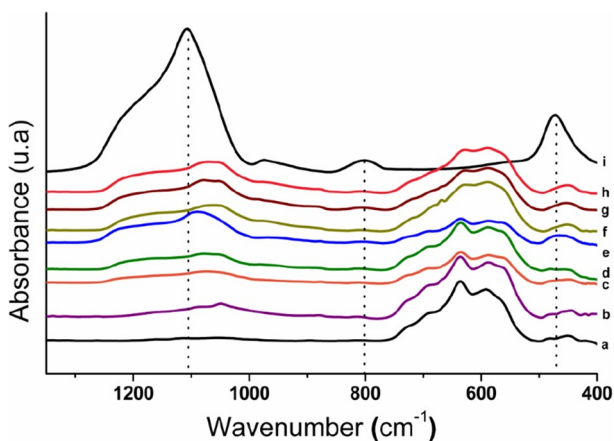
Fig. 4 FTIR spectra of: (a) Fe$_3$O$_4$; (b-h) Fe$_3$O$_4$@SiO$_2$ with different amounts of SiO$_2$ coatings; and (i) SiO$_2$, Reprinted with permission from Ref. [93], Surf. Interfaces (2019), 14 © Copyright Elsevier

Ma et al. [100] have prepared alginate-coated magnetic particles and the binding of magnetite to alginate was emphasized by FTIR analysis by characteristic carboxyl group adsorption bands (from β-(1–4)-ᴅ-mannuronic and α-ʟ-gluronic acid units) around 1610 cm^{-1} and 1410 cm^{-1}. Compared to alginate sample the bands were shifted to lower frequencies indicating the interaction between iron oxide and alginate. Magnetic solid acid catalyst, designed as 12-tungstophosphoric acid loaded on the surface of mesoporous silica supported on magnetite core (Fe$_3$O4@SBA-15@HPW) was synthesized by Zhang et al. [101], as a catalyst for biodiesel production. The successful coating of magnetite was investigated for the Keggin structure of HPW in the FTIR spectra, through the presence of the stretching frequency of P–O in the central PO$_4$ tetrahedron (1120 cm^{-1}), (terminal bands for W=O in the exterior WO6 octahedron (1000 cm^{-1}) and bands for the W–Ob–W and W–Oc–W bridge (879 and 800 cm^{-1}) [101].

Table 7 summarizes wavenumbers, characteristics and functional group of selected groups present on the surface of functionalized magnetite.

Table 7 Selected vibrational assignments and characteristics for magnetite and some of the most common groups present on the surface of functionalized magnetite

Wavenumber (cm^{-1})	Functional group vibrations	Characteristics	Refs.
570–580	Me–O (Fe–O)	Crystalline lattice of Fe$_3$O$_4$	[167–170]
1095 and 1193	S=O	SO$_3$H groups	[171]
800, 1000–1100	Si–O and Si–O-Si	Silica	[101, 172]
1120	P–O	PO$_4$	[101]
1030–1330	C–O	Alcohol group	[173]
1080	C–O–C	Glycols groups	[173]
1400–1500; 1600	C=C	Aromatic ring	[172, 174]
1550–1650	C=N		[174]
1650–1750	C=O	Carbonyl group, carboxylic acid, esters	[112, 175]
2850 and 2950	C–H	Hydrocarbon chains	[173, 174]
1630 broad 3200–3600 broad	OH bending OH stretching	Adsorbed water molecules	[112]
3300–3500	N–H	Amines	[176]

X-ray diffraction (XRD) is one of the most extensively used nondestructive techniques for the characterization of materials that provides information regarding the crystalline structure, lattice parameters, chemical composition, physical properties of materials and crystallite sizes [102]. The information about crystal structure and quantitative phase analyses can be obtained based on the peak intensity and the peak shape gives information about micro strains and crystallite size. If the width of the peaks in XRD patterns is narrow the particles are nanosized [103]. Diffraction data, usually presented as intensity distribution as a function of the 2θ angle, can give several useful information presented in Fig. 5.

The crystallite sizes parameter is estimated using the Scherrer equation (Eq. 6) from the broadening of the most intense peak of an XRD measurement for a specific sample [104].

$$FWHM(2\theta) = \frac{b \cdot \lambda}{D \cdot \cos\theta} \tag{6}$$

The value of the dimension of the crystallite considered as cubes (D) in Eq. 6 can be calculated by Eq. 7:

$$D = \frac{2 \cdot b \cdot \pi}{FWHM(Q)} \tag{7}$$

Here FWHM is the full width of the peak, 2θ is the scattering angle in radians, λ is the wavelength, Q is the magnitude of the scattering vector, b is a constant, which normally takes a value between 0.89 and 0.94 depending on the function

used to fit the peak and *D* is the dimension of the crystallites as if they were cubes, monodisperse in size. Therefore, for different reflections and different crystallite shapes, the interpretation of D must be treated with some care. For polydisperse systems, D is a measure of the volume-averaged crystallite size, which can be determined from Eq. 8:

$$d = \frac{K \cdot \lambda}{B \cdot \cos \theta} \tag{8}$$

Here D is the crystallite average size; K is the shape factor; λ is the x-ray wavelength; B is the instrument broadening (FWHM—full width at half maximum); θ is the theta, half of the Bragg angle (radians).

For magnetite, the crystallite size of the samples is determined by Scherrer equation from the measured width of the 311 peak, which is the most intense one [105]. The composition of the particles can be determined by comparing the position and intensity of the peaks with the reference patterns available from database: ICDD (International Centre for Diffraction Data), previously JCPDS (Joint Committee on Powder Diffraction Standards).

Alfredo Reyes Villegas et al. [25] determined the average crystallite size of magnetite nanoparticles by application of the Scherrer equation to the reflection 311 peak with 2θ ~ 35.5 and it was found to be in the range of 16 nm [25]. The reference pattern for synthesized nanoparticles was the JCDPS Card 19-0629. The crystallinity of the magnetic nanoparticles is assigned to strong and sharp peaks, while the broadening indicates the nanosized of the particles. Similarly, Mascolo et al. [52] noticed that in the XRD patterns, the peak positions shift slightly forward to larger 2θ values with the increasing pH of the synthesis solution. The (311) XRD peak of
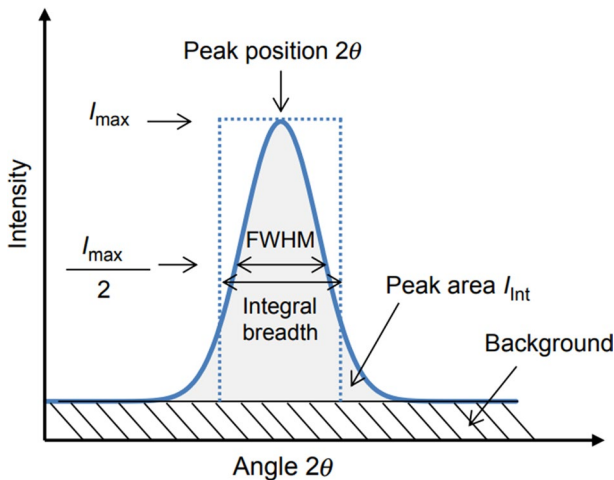

Fig. 5 Graphical representation of diffraction data and information that can be extracted, Reprinted with permission from Ref. [150], *Materials Characterization Using Nondestructive Evaluation (NDE) Methods* (2016) pp. 81–124 © Copyright Elsevier

the products showed the peak shift, indicating that the lattice parameter contracts as the particle size decreases.

For magnetite, the reflection planes with the respective diffraction angles, relative peak intensities and interplanar spacing are shown in Table 8 (according to Shi et al. [106])*.*

An example of XRD pattern of Fe_3O_4 nanoparticles obtained by Predescu et al. [107] is shown in Fig. 6, where the several well-defined reflections can be observed.

The differentiation between magnetite and maghemite on the nanoscale using XRD is difficult because both iron oxides have cubic structure, and their lattice parameters are almost identical. Minor differences in the diffractogram of maghemite exist in the form of a few extra peaks at 210 and 213 (weak intensities) which can possibly be used to distinguish magnetite from maghemite [108]. A method proposed by Kim et al. [109] can be used to identify and quantify mixtures of magnetite-maghemite by scanning the 511 peak (Fig. 7) and resolved through the deconvolution routine. Another possible way to differentiate between magnetite and maghemite is Raman spectroscopy [73] or UV–Vis spectroscopy [110].

Thermal gravimetric analysis (TGA) can provide information concerning the mass and composition of the surface modifiers of the magnetic nanoparticles. With this technique, the sample is heated and the changes in weight are correlated with the sample composition and stability. TGA analysis is extensively utilized to measure the thermal stability, composition, moisture, oxidative stability, and volatile content, kinetics of decomposition, sample dehydration and lifetime.

Soh et al. [111] recorded a TG curve of Fe_3O_4 from 25 to 950 °C, under a nitrogen atmosphere and attributed the three mass losses to (1) the absorbed water molecules (25 °C–200 °C), (2) the physisorption and chemisorption processes occurring at the surface of the magnetite (250 °C–400 °C) and (3) phase transition from magnetite to hematite (500 °C–750 °C). If the thermogravimetric analysis is carried out in air atmosphere, a weight increase assigned to the oxidation of Fe_3O_4 to Fe_2O_3 can be observed from TG curve [112, 113]. The weight increase was observed by Liang and Lu [112] between 140 and 210 °C.

Table 8 X-ray diffraction characteristics of Fe_3O_4 [106]

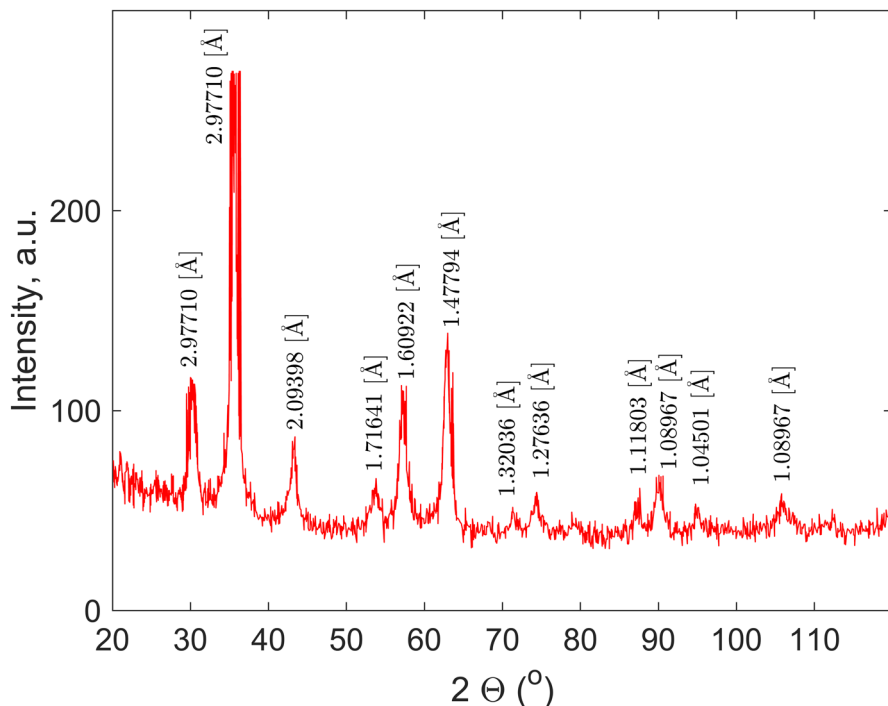| d-spacing	θ (°)	Intensity (relative)	Plane
4.852	18.3	8	111
2.967	0.1	30	220
2.5432	35.3	100	311
2.424	37.1	8	222
2.099	43.1	20	400
1.7146	53.4	10	422
1.6158	56.9	30	511
1.4845	62.5	40	440
1.2807	73.9	10	620
1.093	89.6	20	622

Fig. 6 Example of a XRD pattern for Fe_3O_4 nanoparticles, Reprinted with permission from Ref. [107], Powder Technol (2019), 432 © Copyright Elsevier

Thermogravimetric analysis is essential for the determination of the weight of surfactant covering the particle surface. For instance, magnetite nanoparticles with oleic acid and amphiphilic block copolymers adsorbed on their surface were investigated with a thermogravimetric analyzer. The grafting density of molecules on the surface of the nanoparticles was studied by TGA under the nitrogen atmosphere, with a heating rate of 20 °C/min from 30 to 800 °C [114]. The thermal stability of magnetic materials coated by blends of modified chitosan and poly(quaternary ammonium) salt has been investigated by Ziegler–Ziegler–Borowska et al. [115] using thermogravimetric analysis in air and nitrogen atmosphere, from 20 to 800 °C. In nitrogen atmosphere, TG curve of chitosan showed two degradation moments at 20 °C–160 °C and 160 °C–400 °C ranges attributed to the evolution of water adsorbed by polymer in the first stage, and by the rupture of polysaccharide chains (including dehydration, deamination, deacetylation, breaking of glycoside bonds, and pyranose ring opening), vaporization, and elimination of degradation products, in the second stage. The chemical modification of chitosan was also confirmed by differences in the TG curves of chitosan and modified chitosan [115]. Similarly, Lesiak et al. [116] studied the stability of various magnetite nanoparticles functionalized with carboxyl groups (for example succinic acid, oxalic acid, citric acid) and amino acid (glutamic acid, L-arginine). TG curves were recorded in the temperature range of 30 °C–600 °C.

Fig. 7 X-ray diffraction patterns of (511) peak obtained from mixtures of Fe_3O_4 γ-Fe_2O_3. Reprinted with permission from Ref. [109], *Talanta* (2012), 94 © Copyright Elsevier
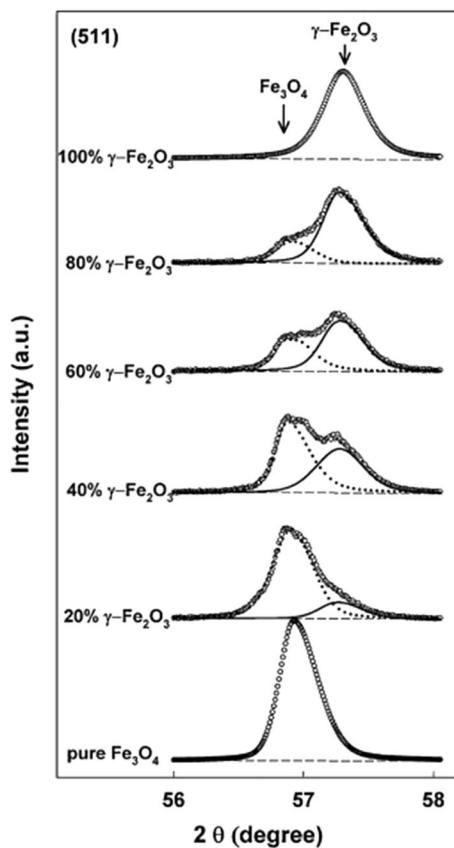
The carboxyl, hydroxyl, carbonyl, and nitrogen groups of chemically adsorbed molecules undergo decomposition, as it was observed in the second temperature region of 150 °C–600 °C.

Dynamic light scattering (DLS) is a widely employed technique to find the size of nanoparticles in colloidal suspensions typically in the sub micrometer range. The size that is measured in DLS is the hydrodynamic diameter and it refers to how a particle diffuses within a fluid. It is calculated using the Stokes–Einstein equation in Eq. (4) [117]:

$$d(H) = \frac{k \cdot T}{3 \cdot \pi \cdot \eta \cdot D} \tag{9}$$

Here: d(H) is the hydrodynamic diameter, D is the translational diffusion coefficient, k is the Boltzmann's constant, T is the absolute temperature and η is the viscosity.

The main factors that affect the diffusion speed of particles are ionic strength of medium, surface structure and the shape of the particles. A low conductivity medium will produce an extended double layer of ions around the particle, reducing

the diffusion speed and resulting in a larger, apparent hydrodynamic diameter. When measuring particle size using DLS, concentration is also an important parameter to consider because it influences scattering of the light and may give inaccurate results. A good standardized method which highlights the sample preparation and analysis is presented in *ISO 22412:2017(E) Particle size analysis — Dynamic light scattering (DLS)* [118]. For an analytical review on the characterization of magnetic particles by DLS, researchers are encouraged to read the paper by Lim et al. [119], who have reviewed the influence of the parameters (suspension concentration, particle shape, colloidal stability and surface coating) on the size value of magnetic nanoparticles obtained by DLS measurements.

Measurement of hydrodynamic diameter is essential in describing particle aggregation, colloidal stability of the particles in various environments and the degree of surface modification of the magnetic nanoparticles. For instance, Arévalo-Cid et al. [120] examined the stability of chitosan-coated Fe_3O_4 nanoparticles over time. Coating was modified by varying the amount of the crosslinker glutaraldehyde and the reaction time between magnetite and chitosan. For DLS measurements they used 0.01 g/l water suspensions of Fe_3O_4 and Fe_3O_4@chitosan crosslinked with different amounts of glutaraldehyde and they observed that the hydrodynamic size of bare magnetite nanoparticles increased over time due to the aggregation of the particles. The aggregation process was also observed for the Fe_3O_4@chitosan samples prepared with small amounts of glutaraldehyde (0.5 ml). Increasing the amount of glutaraldehyde, smaller size of the aggregates was initially observed explained by a better dispersion in water of the samples, as a result of a thicker formed chitosan coating. Even if the chitosan presence improves the initial dispersion of the particles in water, it does not prevent the aggregation of constituent particles over time. [120]. The aggregation of commercially available magnetite nanoparticles (Skyspring Nanomaterials) using DLS was determined as a function of pH, in a pH range of 2–12. Magnetite nanoparticles were dispersed in MilliQ filtered water and the pH was adjusted to the wanted value, using nitric acid or potassium hydroxide. Results indicated that as the pH value increases, the effective diameter increases and the stability decreases. Furthermore, particle aggregation occurred at pH 7.5, the isoelectric point of magnetite [121].

Magnetic nanoparticles coated with a layer of surfactants (e.g.) prevent their agglomeration and keep them stable, but also prevent the particles from not dispersing in aqueous solutions, an important property because for biomedical applications nanoparticles must be water soluble [122]. Gonzales and Krishnan [123] succeeded to make iron oxide nanoparticles soluble in aqueous solutions by coating them with copolymer Pluronic F127. DLS measurements were used to analyze the hydrodynamic diameter of the oleic acid-magnetite nanoparticles before and after the coating and thus, the success of the magnetic nanoparticles transferred in water. The hydrodynamic diameter of the nanoparticles before coating with Pluronic F 127 was analyzed in toluene, because the oleic acid-magnetite nanoparticles were soluble in toluene. After Pluronic F 127 coating, the magnetite nanoparticles were transferred to the water phase and the hydrodynamic diameter was measured in aqueous medium.

X-ray photoelectron spectroscopy (XPS) is a powerful quantitative technique, useful to elucidate the electronic structure, elemental composition, and oxidation states of elements in a material. The main drawbacks of XPS technique are the sample preparation and data collection and interpretation. Baer [124] elaborated a short comprehensive guide with good practices on XPS measurement objectives, sample preparation and analysis approaches when characterizing nanoparticles.

The XPS analysis of mixed iron oxide systems are complex because of peak asymmetries, multiple splitting, shake-up satellite structure and overlapping binding energies [125] and should include corroborating evidence from O 1 s analysis and other analytical techniques. Grosvenor et al. [126] paper is an excellent starting point for qualitative ferrous (Fe^{2+}) and ferric (Fe^{3+}) compounds determination. An XPS analysis of the chemical states of Fe oxides and hydroxides was made by Biesinger et al. [127] and the fitting Fe 2p3/2 parameters in magnetite are presented in Table 9.

A sample with more than three species cannot be accurately fitted. For example, the resulting fit for a mixture of iron oxides components, Fe_3O_4 and Fe_2O_3, is shown in Fig. 8. Because the higher binding energy satellite peaks for Fe_2O_3 are omitted from the fitting, as are the assumed satellites for the Fe_3O_4 components, it causes a slight overestimation of the metal compared to the two oxide components [127].

The XPS technique can also analyze the ligand exchange interactions and surface functionalization of magnetic nanoparticles. The mechanism of arsenate adsorption on a magnetite-doped activated carbon fiber was investigated by Zhang et al. [128] using the XPS technique, by tracking the change in core level peak position of the adsorbents, thus deducing the direction of electron transfer during adsorption. In another report, magnetite nanoparticles coated with L-ascorbic acid (LAA) were investigated by FTIR and XPS to confirm that LAA is capped on the surface of magnetite nanoparticles [129]. The presence of C=O of LAA capped on the surface of magnetite nanoparticles was proved from XPS spectra of the O1 peak (located at 531.8 eV) and from XPS spectrum of Fe2p which had higher binding energy peaks than the reference Fe_3O_4 without LAA. Furthermore, the XPS technique can also distinguish between core–shell and homogeneous alloy structures. Many studies have demonstrated that if particles possessed a core–shell system, the core element would be screened by the shell element, and thus, the compositions in the shell layer become gradually more dominant. The chemical information from the particles surface analyzed by XPS can be used to assess the thickness of the coatings [130, 131].

Scanning electron microscopy (SEM) is excellent for nanoparticles shape and size characterization, and it is one of the most used techniques for this purpose. Sample preparation in SEM analysis is very important because it can result in artefacts that can influence the quality of the results. The ISO 19749:2021—*Nanotechnologies — Measurements of particle size and shape distributions by scanning electron microscopy* [132] provide useful information with examples about nanoparticles morphology and size characterization by SEM technique.

In early years SEM analysis could not distinguish between iron oxide phases (e.g. magnetite, maghemite, hematite or goethite) due to insufficient precision of conventional EDS [133]. Innovative SEMs can analyze different iron oxides if a sufficient number of counts is acquired. John Konopka could differentiate between magnetite,

Table 9 Fe 2p3/2 spectral fitting parameters: binding energy (eV), percentage of total area, FWHM value (eV) in magnetite [127]

Chemical state	Peak 1 (eV)	FWHM (10 eV pass energy)	%	Peak 2 (eV)	FWHM (10 eV pass energy)	%	Peak 3 (eV)	FWHM (10 eV pass energy)	%
Fe $^{2+}$	708.4	1.2	16.6	709.2	1.2	14.8	–	–	–
Fe $^{3+}$	710.2	1.4	23.7	711.2	1.4	17.8	712.3	1.4	12.2
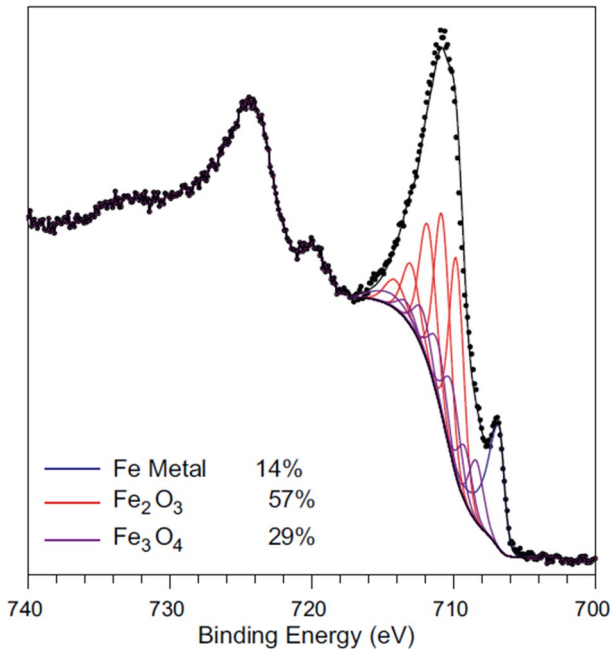
Fig. 8 Curve fitted Fe 2p spectrum of a mixed metal/oxide system of Fe based nanoparticles, Reprinted with permission from Ref. [127], Appl. Surf. Sci (2011), 257 © Copyright Elsevier

hematite and goethite with 350 k counts in the Fe peak.[134], but this can apply for larger particles in μm domain [135].

Transmission electron microscopy (TEM) is another helping tool for magnetic nanoparticles morphological characterization and size and size distribution determination in order to define the unique set of physical properties such as magnetic, optical, catalytic and so on (measured/analyzed with other techniques) [136, 137]. Like SEM analysis, the ISO 21363:2020—*Nanotechnologies—Measurements of particle size and shape distributions by transmission electron microscopy* [138] provide useful information on capturing, measuring and analyzing transmission electron microscopy images to obtain particle size and shape distributions in the nanoscale range. Compared to SEM analysis, with the help of TEM we can get information about the core structure too, and not only about the external structure, which is very important because the magnetic nanoparticles may have different behavior for varied core and coating dimensions [91].

Deng et al. [139] used TEM analysis to evaluate how the solvent used in preparation of silica coated magnetic nanoparticles (alcohol type: methanol, ethanol i-propanol and n–propanol) influences the coating, size and morphology of silica coated magnetite particles. Based on TEM results, they concluded that ethanol is the best candidate alcohol to obtain uniform silica coated magnetite particles and they associated thus to the polarity of the alcohol. The decrease of polarity of alcohol, (from methanol to ethanol to i-propanol to n-propanol) conducted to larger clusters of more irregular particles. TEM is also capable of distinguishing between core and shell(s). The formation

of core–shell nanoparticle may be observed from the differences in contrast to typical TEM micrograph. ZnO layer of about 0.25 nm, of spherical core–shell Fe_3O_4@ZnO nanoparticle was observed and measured using TEM by Gupta et al. [140]. Similar results was also observed by Faaliyan et al. [141] in Fe_3O_4@SiO_2 core–shell nanoparticles with the mean size of the cores of about 20 nm and the shell thickness, 2.5 nm. Organic surface functionalization compounds, such as polystyrene (PS) or polyacrylic acid (PAA) could also be observed in TEM micrograph [106]. Fig. 9 shows a typical TEM micrograph of a core–shell Fe_3O_4@SiO_2 (nonporous)@ SiO_2 (mesoporous) nanoparticle, where the black core is Fe_3O_4, the dark grey shell is nonporous SiO_2 layer ($nSiO_2$) and the lighter shell is the mesoporous SiO_2 layer ($mSiO_2$) [142].

Magnetometry techniques with the help of vibrating sample magnetometer *(VSM)* () or superconducting quantum interference device *(SQUID)* () are the most used to measure the magnetic behavior and they give quantifiable results on the magnetic properties of a material. The measured properties are the magnetization (M) as a function of applied field (H), temperature and time.

The saturation magnetization (Ms) of bulk magnetite at room temperature is 92–100 emu/g. The saturation magnetization of magnetite nanoparticles is smaller than the bulk magnetite value and it decreases with the reduction of the particle size. From the analyzed literature it was found that iron oxide nanoparticles often display superparamagnetism.

Superparamagnetism is one type of magnetism that occurs in ferromagnetic and ferrimagnetic nanostructures with size range of 20 nm or less. Due to the presence of single domain state the nanoparticles behave magnetically only under the influence of an external magnetic field and are rendered inactive once removed- they retain no remnant magnetization upon the removal of the external magnetic field [143, 144], The reduction in particle size of magnetite and maghemite, from bulk to nanoscale, reduces the

Fig. 9 TEM micrographs of Fe_3O_4@nonporous SiO_2 @ mesoporous SiO_2 core–shell nanoparticle, Reprinted with permission from Ref [142], JACS (2008), 130 Copyright American Chemical Society
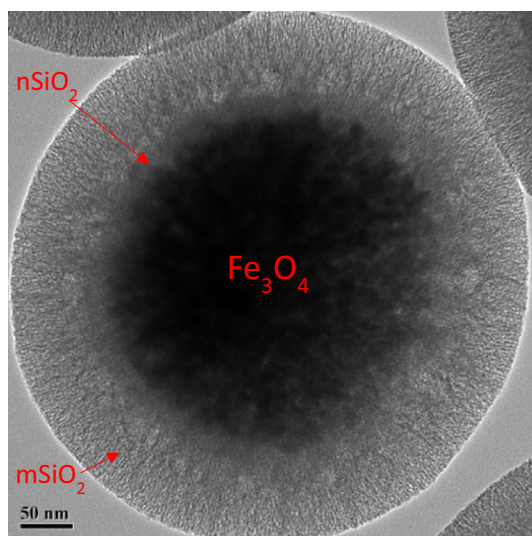
quantity of exchange-coupled spins that rebels magnetic reorientation spontaneously, resulting in superparamagnetic behaviour [145].

Maity et al. [146] used VSM and SQUID magnetometry to carry out the magnetic measurements of a stable aqueous magnetite suspension based on Fe_3O_4 functionalized with tri(ethylene glycol)-TREG. Their magnetization results showed a saturation magnetization of 65 emu/g and a superparamagnetic behavior of the magnetite nanoparticles indicated by zero coercivity and zero remanence on the magnetization curves. The blocking temperature of the particles was determined to be 100 K, below this temperature the particles are ferromagnetic. Yau and colleagues prepared dispersions of magnetite covered with L-ascorbic acid and the magnetic behavior was demonstrated by VSM. The saturation magnetization (Ms) of magnetite particles with L-ascorbic acid was smaller than that of bare magnetite, but the particles maintained their superparamagnetism property as evidenced by the lack of hysteresis loop [129]. Generally, the saturation magnetization of the functionalized magnetite is smaller than that of the bare one, due to the decrease of the effective atoms contributing to the magnetism of the samples [147, 148]. Cîrcu et al. [149] succeeded in enhancing the saturation magnetization of the starting magnetite nanoparticles using α-hydroxy acids (glycolic acid, malic acid, and mandelic acid) stabilizers able to form chelate complexes with the magnetite.

Sandler et al. [91] published a paper on magnetic nanoparticle characterization, which is suggested to researchers new to the field but not limited to, that highlight 'best practices' for structural, chemical, and mainly magnetic characterization.

Summary and perspectives

There is a great potential for the application of magnetite nanoparticles and a lot of research studies have been conducted to synthesize the best material for targeted application. This paper highlighted the features of the coprecipitation method, which is the most widely used method for magnetite nanoparticles production. The parameters influencing the process such as pH of the solution and the precipitating agent, temperature, ion precursor, ionic strength, and stirring rate have been discussed, exemplified, and summarized to ensure that young and senior researchers understand the process and may select the most suitable reaction conditions for their samples considering the field of application.

From the selected literature, it results that the size, shape, saturation magnetization and composition (iron oxide phase) of the resulting nanoparticles are very much dependent upon the presented parameters:

- Usually, magnetite nanoparticles are prepared in a pH value between 9 and 13.
- Smaller magnetite nanoparticles are obtained at higher pH values.
- A strong alkaline medium (such as NaOH, KOH, or LiOH) can lead to formation of nonmagnetic iron components, so to avoid this, weak bases such as NH_4OH or Na_2CO_3 are recommended.
- Magnetite nanoparticles with high purity are obtained at room temperature and at higher temperature too (up to 85 °C), but usually at high temperatures larger particles can be produced with higher saturation magnetization values.

- The most used anions of iron salts consist of chloride, sulfate, and nitrate.
- The growth of oxide nanoparticles in aqueous solution can be controlled by controlling the ionic strength of the reaction solution- the increase in ionic strength results in reducing the size of the magnetic nanoparticles.
- At fast stirring speed the growth of the particles is reduced, resulting in smaller size particles.

To ensure they best describe these materials a comprehensive summary of magnetic nanoparticle characterization methods was presented, emphasizing their advantages and limitations.

In order to prevent magnetite oxidation, most of the studies are conducted in an inert atmosphere or in the presence of protective agents. Future work in this area must be focused on the research of the stability of bare, or surface functionalized magnetic nanoparticles, in time and in the media, they are intended to be used. Many studies present the stability of synthesized magnetic nanoparticles by zeta potential measurements. While zeta potential is a good indication of particles stability in suspensions, tests regarding chemical stability or the stability of the particles over time should be more often addressed.

Although many papers are dedicated to the synthesis of magnetic nanoparticles by coprecipitation, challenges remain in different aspects of working with this. The influence of mixing order of the reactants and the contact time of the ions, before adding the precipitating agent, on structural and magnetic properties of the particles had not been clearly demonstrated.

Some outlooks on further developments of magnetic nanoparticles using coprecipitation method, include study of the influence of shell thickness of magnetic core–shell particles and large-scale (industrially) production of ideal functionalized iron oxide materials. The "LaMer model" is often named to interpret the size distributions of the synthesized iron oxide nanoparticles. For iron oxide nanoparticles, the model is often cited as a diagrammatic drawing and the description of the model is only associated by words. A further perspective on mechanism elucidation is the experimental evidence that LaMer model is f the experimental nucleation kinetics data of iron oxide nanoparticles.

Data availability No new data was created or analyzed in this study. Data sharing is not applicable to this article.

Declarations

Conflicts of interest There are no conflicts to declare.

References

1. Arteaga-Díaz SJ, Meramo-Hurtado SI, León-Pulido J, Zuorro A, González-Delgado AD (2019) Environmental assessment of large scale production of magnetite (Fe_3O_4) nanoparticles via coprecipitation. Appl Sci 9:1–10. https://doi.org/10.3390/app9081682
2. Ebner AD, Ritter JA, Navratil JD (2001) Adsorption of cesium, strontium, and cobalt ions on magnetite and a magnetite-silica composite. Ind Eng Chem Res 40:1615–1623. https://doi.org/10.1021/ie000695c
3. Park H, May A, Portilla L, Dietrich H, Munch F, Rejek T, Sarcletti M, Banspach L, Zahn D, Halik M (2020) Magnetite nanoparticles as efficient materials for removal of glyphosate from water. Nat Sustain 3:129–135. https://doi.org/10.1038/s41893-019-0452-6
4. Matei E, Predescu A, Dragan C, Pantilimon C, Predescu C (2017) Characterization of magnetic nanoiron oxides for the removal of metal ions from aqueous solution. Anal Lett 50:2822–2838. https://doi.org/10.1080/00032719.2016.1257016
5. Predescu A, Matei E, Predescu A, Berbecaru A, Sohaciu M, Predescu C (2016) Removal of hexavalent chromium from waters by means of a TiO_2-Fe_3O_4 nanocomposite. Environ Eng Manag J 15:989–994. https://doi.org/10.30638/eemj.2016.108
6. Matei E, Predescu AM, Coman G, Balanescu M, Sohaciu M, Predescu C, Favier L, Niculescu M (2016) Magnetic nanoparticles used in envinronmental engineering for Pb and Zn removal. Environ Eng Manag J 15:1019–1025. https://doi.org/10.30638/eemj.2016.112
7. Matei E, Predescu C, Badanoiu A, Predescu A, Ficai D (2015) Application of magnetite nanoparticles as adsorbent for Cr, Cd, Ni and Cu from aqueous solutions. Environ Eng Manag J 14:1001–1010. https://doi.org/10.30638/eemj.2015.110
8. Mohammadi M, Pourseyed AF (2021) Magnetite Fe_3O_4 surface as an effective drug delivery system for cancer treatment drugs: density functional theory study. J Biomol Struct Dyn 39:2798–2805. https://doi.org/10.1080/07391102.2020.1754915
9. Chandra S, Mehta S, Nigam S, Bahadur D (2010) Dendritic magnetite nanocarriers for drug delivery applications. New J Chem 34:648–655. https://doi.org/10.1039/b9nj00609e
10. Bauer LM, Situ SF, Griswold MA, Samia AC (2016) High-performance iron oxide nanoparticles for magnetic particle imaging - guided hyperthermia (hMPI). Nanoscale 8:12162–12169. https://doi.org/10.1039/c6nr01877g
11. Dey K, Karmakar G, Upadhyay M, Ghosh P (2020) Polyacrylate-magnetite nanocomposite as a potential multifunctional additive for lube oil. Sci Rep 10:19151. https://doi.org/10.1038/s41598-020-76246-4
12. Tudorache M, Opris C, Cojocaru B, Apostol NG, Tirsoaga A, Coman SM, Parvulescu VI, Duraki B, Krumeich F, van Bokhoven JA (2018) Highly efficient, easily recoverable, and recyclable re-SiO_2-Fe_3O_4 catalyst for the fragmentation of lignin. Acs Sustain Chem Eng 6:9606–9618. https://doi.org/10.1021/acssuschemeng.7b04294
13. Kazemi M, Ghobadi M (2017) Magnetically recoverable nano-catalysts in sulfoxidation reactions. Nanotechnol Rev 6:549–571. https://doi.org/10.1515/ntrev-2016-0113
14. Oprescu EE, Enascuta CE, Doukeh R, Calin C, Lavric V (2021) Characterizing and using a new bi-functional catalyst to sustainably synthesize methyl levulinate from biomass carbohydrates. Renew Energ 176:651–662. https://doi.org/10.1016/j.renene.2021.05.120
15. Salimi P, Norouzi O, Pourhosseini SEM (2019) Two-step synthesis of nanohusk Fe_3O_4 embedded in 3D network pyrolytic marine biochar for a new generation of anode materials for lithium-ion batteries. J Alloys Compd 786:930–937. https://doi.org/10.1016/j.jallcom.2019.02.048
16. Jaime J, Rangel G, Munoz-Bonilla A, Mayoral A, Herrasti P (2017) Magnetite as a platform material in the detection of glucose, ethanol and cholesterol. Sensor Actuat B 238:693–701. https://doi.org/10.1016/j.snb.2016.07.059
17. Polatoğlu İ (2019) Electrochemical sensing platform based on tyrosinase immobilized magnetite chitosan nanobiocomposite film and its application as catechol biosensor. J Electrochem Soc 166:B1620–B1629. https://doi.org/10.1149/2.1041915jes
18. Dubey V, Kain V (2018) Synthesis of magnetite by coprecipitation and sintering and its characterization. Mater Manuf Process 33:835–839. https://doi.org/10.1080/10426914.2017.1401720
19. Unni M, Uhl AM, Savliwala S, Savitzky BH, Dhavalikar R, Garraud N, Arnold DP, Kourkoutis LF, Andrew JS, Rinaldi C (2017) Thermal decomposition synthesis of iron oxide nanoparticles

with diminished magnetic dead layer by controlled addition of oxygen. ACS Nano 11:2284–2303. https://doi.org/10.1021/acsnano.7b00609

20. Drmota A, Drofenik M, Koselj J, Znidarsic A (2012) Microemulsion method for synthesis of magnetic oxide nanoparticles. In: Najjar R, Hrsg. Microemulsions— an introduction to properties and applications. Intech Open

21. Lemine OM, Omri K, Zhang B, El Mir L, Sajieddine M, Alyamani A, Bououdina M (2012) Sol–gel synthesis of 8 nm magnetite (Fe_3O_4) nanoparticles and their magnetic properties. Superlatt Microstruct 52:793–799. https://doi.org/10.1016/j.spmi.2012.07.009

22. Ahmadi S, Chia CH, Zakaria S, Saeedfar K, Asim N (2012) Synthesis of Fe_3O_4 nanocrystals using hydrothermal approach. J Magn Magn Mater 324:4147–4150. https://doi.org/10.1016/j.jmmm.2012.07.023

23. Cabrera L, Gutierrez S, Menendez N, Morales MP, Heffasti P (2008) Magnetite nanoparticles: electrochemical synthesis and characterization. Electrochim Acta 53:3436–3441. https://doi.org/10.1016/j.electacta.2007.12.006

24. Bharde A, Wani A, Shouche Y, Joy PA, Prasad BL, Sastry M (2005) Bacterial aerobic synthesis of nanocrystalline magnetite. J Am Chem Soc 127:9326–9327. https://doi.org/10.1021/ja0508469

25. Alfredo Reyes Villegas V, De León I, Ramírez J, Hernandez Guevara E, Perez Sicairos S, Angelica Hurtado Ayala L, Landeros SB (2020) Synthesis and characterization of magnetite nanoparticles for photocatalysis of nitrobenzene. J Saudi Chem Soc 24:223–235. https://doi.org/10.1016/j.jscs.2019.12.004

26. Andrade AL, Valente MA, Ferreira JMF, Fabris JD (2012) Preparation of size-controlled nanoparticles of magnetite. J Magn Magn Mater 324:1753–1757. https://doi.org/10.1016/j.jmmm.2011.12.033

27. Zhu N, Ji H, Yu P, Niu J, Farooq MU, Akram MW, Udego IO, Li H, Niu X (2018) Surface modification of magnetic iron oxide nanoparticles. Nanomaterials. https://doi.org/10.3390/nano8100810

28. Popescu RC, Andronescu E, Vasile BS (2019) Recent advances in magnetite nanoparticle functionalization for nanomedicine. Nanomaterials. https://doi.org/10.3390/nano9121791

29. Daoush WM (2017) Co-precipitation and magnetic properties of magnetite nanoparticles for potential biomedical applications. J Nanomed Res. https://doi.org/10.15406/jnmr.2017.05.00118

30. Santoso UT, Abdullah MDR, Ariyani D, Waskito J (2021) Room temperature synthesis of magnetite particles by an oil membrane layer-assisted reverse co-precipitation approach. Adv Mater Res 1162:41–46. https://doi.org/10.4028/www.scientific.net/AMR.1162.41

31. Ajinkya N, Yu X, Kaithal P, Luo H, Somani P, Ramakrishna S (2020) Magnetic iron oxide nanoparticle (IONP) synthesis to applications: present and future. Materials 13:1–35. https://doi.org/10.3390/ma13204644

32. Krishnan KM (2010) Biomedical nanomagnetics: A spin through possibilities in imaging, diagnostics, and therapy. IEEE Trans Magn 46:2523–2558. https://doi.org/10.1109/TMAG.2010.2046907

33. Mylkie K, Nowak P, Rybczynski P, Ziegler-Borowska M (2021) Polymer-coated magnetite nanoparticles for protein immobilization. Materials 14:248. https://doi.org/10.3390/ma14020248

34. Teja AS, Koh P-Y (2009) Synthesis, properties, and applications of magnetic iron oxide nanoparticles. Prog Cryst Growth Charact Mater 55:22–45. https://doi.org/10.1016/j.pcrysgrow.2008.08.003

35. Majewski P, Thierry B (2007) Functionalized magnetite nanoparticles—synthesis, properties, and bio-applications. Crit Rev Solid State Mater Sci 32:203–215. https://doi.org/10.1080/10408430701776680

36. Kozlenko DP, Dubrovinsky LS, Kichanov SE, Lukin EV, Cerantola V, Chumakov AI, Savenko BN (2019) Magnetic and electronic properties of magnetite across the high pressure anomaly. Sci Rep 9:4464. https://doi.org/10.1038/s41598-019-41184-3

37. Narang SB, Pubby K (2021) Nickel spinel ferrites: a review. J Magn Magn Mater 519:167163. https://doi.org/10.1016/j.jmmm.2020.167163

38. Benitez MJ, Mishra D, Szary P, Badini Confalonieri GA, Feyen M, Lu AH, Agudo L, Eggeler G, Petracic O, Zabel H (2011) Structural and magnetic characterization of self-assembled iron oxide nanoparticle arrays. J Phys Condens Matter 23:126003. https://doi.org/10.1088/0953-8984/23/12/126003

39. Peternele WS, Fuentes VM, Fascineli ML, da Silva JR, Silva RC, Lucci CM, de Azevedo RB (2014) Experimental investigation of the coprecipitation method: An approach to obtain magnetite and maghemite nanoparticles with improved properties. J Nanomater 2014:682985. https://doi.org/10.1155/2014/682985

40. Grau-Crespo R, Al-Baitai AY, Saadoune I, De Leeuw NH (2010) Vacancy ordering and electronic structure of gamma-Fe_2O_3 (maghemite): a theoretical investigation. J Phys Condens Matter 22:255401. https://doi.org/10.1088/0953-8984/22/25/255401

41. Doukeh R, Râpă M, Matei E, Prodan D, Győrgy R, Trifoi A, Banu I (2023) An evaluation of glycerol acetalization with benzaldehyde over a ferromagnetic heteropolyacid catalyst. Catal 13:1–21. https://doi.org/10.3390/catal13040782

42. Peng J, Zou F, Liu L, Tang L, Yu L, Chen W, Liu H, Tang J-b, Wu L-x (2008) Preparation and characterization of PEG-PEI/Fe3O4 nano-magnetic fluid by co-precipitation method. Trans Nonferrous Met Soc 18:393–398. https://doi.org/10.1016/S1003-6326(08)60069-2

43. Cabrera L, Gutierrez S, Menendez N, Morales MP, Herrasti P (2008) Magnetite nanoparticles: electrochemical synthesis and characterization. Electrochim Acta 53:3436–3441. https://doi.org/10.1016/j.electacta.2007.12.006

44. Pichon BP, Gerber O, Lefevre C, Florea I, Fleutot S, Baaziz W, Pauly M, Ohlmann M, Ulhaq C, Ersen O, Pierron-Bohnes V, Panissod P, Drillon M, Begin-Colin S (2011) Microstructural and magnetic investigations of wüstite-spinel core-shell cubic-shaped nanoparticles. Chem Mater 23:2886–2900. https://doi.org/10.1021/cm2003319

45. Vargas-Ortiz JR, Gonzalez C, Esquivel K (2022) Magnetic iron nanoparticles: synthesis, surface enhancements, and biological challenges. Processes 10:1–29. https://doi.org/10.3390/pr10112282

46. Sharafi Z, Bakhshi B, Javidi J, Adrangi S (2018) Synthesis of silica-coated iron oxide nanoparticles: preventing aggregation without using additives or seed pretreatment. Iran J Pharm Res 17:386–395

47. Na K-H, Kim W-T, Park D-C, Shin H-G, Lee S-H, Park J, Song T-H, Choi W-Y (2018) Fabrication and characterization of the magnetic ferrite nanofibers by electrospinning process. Thin Solid Films 660:358–364. https://doi.org/10.1016/j.tsf.2018.06.018

48. Ying T-Y, Yiacoumi S, Tsouris C (2002) An electrochemical method for the formation of magnetite particles. J Dispers Sci Technol 23:569–576. https://doi.org/10.1081/DIS-120014025

49. Franger S, Berthet P, Berthon J (2004) Electrochemical synthesis of Fe_3O_4 nanoparticles in alkaline aqueous solutions containing complexing agents. J Solid State Electrochem 8:218–223. https://doi.org/10.1007/s10008-003-0469-6

50. Jordan A, Scholz R, Wust P, Fähling H, Roland F (1999) Magnetic fluid hyperthermia (MFH): cancer treatment with AC magnetic field induced excitation of biocompatible superparamagnetic nanoparticles. J Magn Magn Mater 201:413–419. https://doi.org/10.1016/S0304-8853(99)00088-8

51. Maity D, Agrawal DC (2007) Synthesis of iron oxide nanoparticles under oxidizing environment and their stabilization in aqueous and non-aqueous media. J Magn Magn Mater 308:46–55. https://doi.org/10.1016/j.jmmm.2006.05.001

52. Mascolo MC, Pei Y, Ring TA (2013) Room temperature co-precipitation synthesis of magnetite nanoparticles in a large pH window with different bases. Materials 6:5549–5567. https://doi.org/10.3390/ma6125549

53. LaGrow AP, Besenhard MO, Hodzic A, Sergides A, Bogart LK, Gavriilidis A, Thanh NTK (2019) Unravelling the growth mechanism of the co-precipitation of iron oxide nanoparticles with the aid of synchrotron X-Ray diffraction in solution. Nanoscale 11:6620–6628. https://doi.org/10.1039/c9nr00531e

54. Blanco-Andujar C, Ortega D, Pankhurst QA, Thanh NTK (2012) Elucidating the morphological and structural evolution of iron oxide nanoparticles formed by sodium carbonate in aqueous medium. J Mater Chem 22:12498–12506. https://doi.org/10.1039/c2jm31295f

55. Ahn T, Kim JH, Yang HM, Lee JW, Kim JD (2012) Formation pathways of magnetite nanoparticles by coprecipitation method. J Phys Chem C 116:6069–6076. https://doi.org/10.1021/jp211843g

56. LaMer VK, Dinegar RH (2002) Theory, production and mechanism of formation of monodispersed hydrosols. J Am Chem Soc 72:4847–4854. https://doi.org/10.1021/ja01167a001

57. Anik MI, Hossain MK, Hossain I, Mahfuz AMUB, Rahman MT, Ahmed I (2021) Recent progress of magnetic nanoparticles in biomedical applications: a review. Nano Select 2:1146–1186. https://doi.org/10.1002/nano.202000162

58. Gnanaprakash G, Mahadevan S, Jayakumar T, Kalyanasundaram P, Philip J, Raj B (2007) Effect of initial pH and temperature of iron salt solutions on formation of magnetite nanoparticles. Mater Chem Phys 103:168–175. https://doi.org/10.1016/j.matchemphys.2007.02.011

59. Gribanov NM, Bibik EE, Buzunov OV, Naumov VN (1990) Physico-chemical regularities of obtaining highly dispersed magnetite by the method of chemical condensation. J Magn Magn Mater 85:7–10. https://doi.org/10.1016/0304-8853(90)90005-b

60. Niu JM, Zheng ZG (2014) Effect of temperature on Fe_3O_4 magnetic nanoparticles prepared by coprecipitation method. Adv Mater Res 900:172–176. https://doi.org/10.4028/www.scientific.net/AMR.900.172

61. Petcharoen K, Sirivat A (2012) Synthesis and characterization of magnetite nanoparticles via the chemical co-precipitation method. Mater Sci Eng B 177:421–427. https://doi.org/10.1016/j.mseb.2012.01.003

62. Saragi T, Depi BL, Butarbutar S, Permana B, Risdiana. (2018) The impact of synthesis temperature on magnetite nanoparticles size synthesized by co-precipitation method. J Phys Conf Ser 1013:012190. https://doi.org/10.1088/1742-6596/1013/1/012190

63. Meng HN, Zhang ZZ, Zhao FX, Qiu T, Yang JD (2013) Orthogonal optimization design for preparation of Fe_3O_4 nanoparticles via chemical coprecipitation. Appl Surf Sci 280:679–685. https://doi.org/10.1016/j.apsusc.2013.05.041

64. Yazid NA, Joon YC (2019) Co-precipitation synthesis of magnetic nanoparticles for efficient removal of heavy metal from synthetic wastewater. AIP Conf Proc 2124:020019. https://doi.org/10.1063/1.5117079

65. Jolivet JP, Froidefond C, Pottier A, Chaneac C, Cassaignon S, Tronc E, Euzen P (2004) Size tailoring of oxide nanoparticles by precipitation in aqueous medium a semi-quantitative modelling. J Mater Chem 14:3281–3288. https://doi.org/10.1039/b407086k

66. Yazdani F, Seddigh M (2016) Magnetite nanoparticles synthesized by co-precipitation method: the effects of various iron anions on specifications. Mater Chem Phys 184:318–323. https://doi.org/10.1016/j.matchemphys.2016.09.058

67. Iwasaki T, Mizutani N, Watano S, Yanagida T, Kawai T (2010) Size control of magnetite nanoparticles by organic solvent-free chemical coprecipitation at room temperature. J Exp Nanosci 5:251–262. https://doi.org/10.1080/17458080903490731

68. Roth HC, Schwaminger SP, Schindler M, Wagner FE, Berensmeier S (2015) Influencing factors in the CO-precipitation process of superparamagnetic iron oxide nano particles: a model based study. J Magn Magn Mater 377:81–89. https://doi.org/10.1016/j.jmmm.2014.10.074

69. Herea DD, Chiriac H, Lupu N (2011) Preparation and characterization of magnetic nanoparticles with controlled magnetization. J Nanopart Res 13:4357–4369. https://doi.org/10.1007/s11051-011-0385-0

70. Yu WG, Zhang TL, Qiao XJ, Zhang JG, Yang L (2007) Effects of synthetical conditions on octahedral magnetite nanoparticles. Mat Sci Eng B 136:101–105. https://doi.org/10.1016/j.mseb.2006.08.030

71. Valenzuela R, Fuentes MC, Parra C, Baeza J, Duran N, Sharma SK, Knobel M, Freer J (2009) Influence of stirring velocity on the synthesis of magnetite nanoparticles (Fe3O4) by the co-precipitation method. J Alloys Compd 488:227–231. https://doi.org/10.1016/j.jallcom.2009.08.087

72. Fadli A, Komalasari AA, Iwantono R, Addabsi AS (2019) Synthesis of magnetite nanoparticles via co-precipitation method. Iop Conf Ser-Mat Sci 622:012013. https://doi.org/10.1088/1757-899x/622/1/012013

73. Schwaminger SP, Syhr C, Berensmeier S (2020) Controlled synthesis of magnetic iron oxide nanoparticles: magnetite or maghemite? Crystals 10:214. https://doi.org/10.3390/cryst10030214

74. Forge D, Roch A, Laurent S, Tellez H, Gossuin Y, Renaux F, Vander Elst L, Muller RN (2008) Optimization of the synthesis of superparamagnetic contrast agents by the design of experiments method. J Phys Chem C 112:19178–19185. https://doi.org/10.1021/jp803832k

75. Ibarra-Sánchez Jd, Preciado-Rojas Y (2016) Effect of operating parameters in the synthesis of magnetic nanoparticles for biomedical applications using a design of experiments 2k. Nova Scientia 8:157–180. https://doi.org/10.21640/ns.v8i17.575

76. Rahmawati R, Permana MG, Harison B, Nugraha YB, Suyatman KD (2017) Optimization of frequency and stirring rate for synthesis of magnetite (Fe_3O_4) nanoparticles by using coprecipitation-ultrasonic irradiation methods. Procedia Eng 170:55–59. https://doi.org/10.1016/j.proeng.2017.03.010

77. Ansari MJ, Kadhim MM, Hussein BA, Lafta HA, Kianfar E (2022) Synthesis and stability of magnetic nanoparticles. Bionanoscience 12:627–638. https://doi.org/10.1007/s12668-022-00947-5

78. Kharisov BI, Dias HVR, Kharissova OV, Vazquez A, Pena Y, Gomez I (2014) Solubilization, dispersion and stabilization of magnetic nanoparticles in water and non-aqueous solvents: recent trends. RSC Adv 4:45354–45381. https://doi.org/10.1039/c4ra06902a

79. Jose Chirayil C, Abraham J, Kumar Mishra R, George SC, Thomas S (2017) Instrumental techniques for the characterization of nanoparticles. In: Thomas S, Thomas R, Zachariah AK et al (eds)

Thermal and rheological measurement techniques for nanomaterials characterization. Elsevier, Amsterdam, pp 1–36

80. Xiong Z, Li SH, Xia YZ (2016) Highly stable water-soluble magnetic nanoparticles synthesized through combined co-precipitation, surface-modification, and decomposition of a hybrid hydrogel. New J Chem 40:9951–9957. https://doi.org/10.1039/c6nj02051h

81. Yu SM, Laromaine A, Roig A (2014) Enhanced stability of superparamagnetic iron oxide nanoparticles in biological media using a pH adjusted-BSA adsorption protocol. J Nanopart Res 16:2484. https://doi.org/10.1007/s11051-014-2484-1

82. Alterary SS, AlKhamees A (2021) Synthesis, surface modification, and characterization of $Fe_3O_4@SiO_2$ core@shell nanostructure. Green Process Synth 10:384–391. https://doi.org/10.1515/gps-2021-0031

83. Hui C, Shen C, Tian J, Bao L, Ding H, Li C, Tian Y, Shi X, Gao HJ (2011) Core-shell $Fe_3O_4@SiO_2$ nanoparticles synthesized with well-dispersed hydrophilic Fe_3O_4 seeds. Nanoscale 3:701–705. https://doi.org/10.1039/c0nr00497a

84. Karimi Pasandideh E, Kakavandi B, Nasseri S, Mahvi AH, Nabizadeh R, Esrafili A, Rezaei KR (2016) Silica-coated magnetite nanoparticles core-shell spheres ($Fe_3O_4@SiO_2$) for natural organic matter removal. J Environ Health Sci Eng 14:21. https://doi.org/10.1186/s40201-016-0262-y

85. Bae H, Ahmad T, Rhee I, Chang Y, Jin SU, Hong S (2012) Carbon-coated iron oxide nanoparticles as contrast agents in magnetic resonance imaging. Nanoscale Res Lett 7:44. https://doi.org/10.1186/1556-276X-7-44

86. Xu C, Sun S (2013) New forms of superparamagnetic nanoparticles for biomedical applications. Adv Drug Deliv Rev 65:732–743. https://doi.org/10.1016/j.addr.2012.10.008

87. Wulandari IO, Mardila VT, Santjojo DJDH, Sabarudin A (2018) Preparation and characterization of chitosan-coated Fe_3O_4 nanoparticles using ex-situ co-precipitation method and tripolyphosphate/sulphate as dual crosslinkers. IOP Conf Ser 299:012064. https://doi.org/10.1088/1757-899x/299/1/012064

88. Sirivat A, Paradee N (2019) Facile synthesis of gelatin-coated Fe_3O_4 nanoparticle: effect of pH in single-step co-precipitation for cancer drug loading. Mater Design 181:107942. https://doi.org/10.1016/j.matdes.2019.107942

89. Can HK, Kavlak S, ParviziKhosroshahi S, Guner A (2018) Preparation, characterization and dynamical mechanical properties of dextran-coated iron oxide nanoparticles (DIONPs). Artif Cells Nanomed Biotechnol 46:421–431. https://doi.org/10.1080/21691401.2017.1315428

90. Castelló J, Gallardo M, Busquets MA, Estelrich J (2015) Chitosan (or alginate)-coated iron oxide nanoparticles: a comparative study. Colloids Surf A: Physicochem Eng 468:151–158. https://doi.org/10.1016/j.colsurfa.2014.12.031

91. Sandler SE, Fellows B, Mefford OT (2019) Best practices for characterization of magnetic nanoparticles for biomedical applications. Anal Chem 91:14159–14169. https://doi.org/10.1021/acs.analchem.9b03518

92. Namduri H, Nasrazadani S (2008) Quantitative analysis of iron oxides using fourier transform infrared spectrophotometry. Corros Sci 50:2493–2497. https://doi.org/10.1016/j.corsci.2008.06.034

93. de Mendonça ESDT, de Faria ACB, Dias SCL, Aragón FFH, Mantilla JC, Coaquira JAH, Dias JA (2019) Effects of silica coating on the magnetic properties of magnetite nanoparticles. Surf Interfaces 14:34–43. https://doi.org/10.1016/j.surfin.2018.11.005

94. Xie SB, Zhang BL, Wang L, Wang J, Li X, Yang G, Gao FB (2015) Superparamagnetic iron oxide nanoparticles coated with different polymers and their MRI contrast effects in the mouse brains. Appl Surf Sci 326:32–38. https://doi.org/10.1016/j.apsusc.2014.11.099

95. Predescu AM, Matei E, Berbecaru AC, Pantilimon C, Dragan C, Vidu R, Predescu C, Kuncser V (2018) Synthesis and characterization of dextran-coated iron oxide nanoparticles. R Soc Open Sci 5:171525. https://doi.org/10.1098/rsos.171525

96. Díaz-Hernández A, Gracida J, García-Almendárez BE, Regalado C, Núñez R, Amaro-Reyes A (2018) Characterization of magnetic nanoparticles coated with chitosan: a potential approach for enzyme immobilization. J Nanomater 2018:1–11. https://doi.org/10.1155/2018/9468574

97. Bar-Shir A, Avram L, Yariv-Shoushan S, Anaby D, Cohen S, Segev-Amzaleg N, Frenkel D, Sadan O, Offen D, Cohen Y (2014) Alginate-coated magnetic nanoparticles for noninvasive MRI of extracellular calcium. NMR Biomed 27:774–783. https://doi.org/10.1002/nbm.3117

98. Modrogan C, Caprarescu S, Dancila AM, Orbulet OD, Grumezescu AM, Purcar V, Raditoiu V, Fierascu RC (2021) Modified composite based on magnetite and polyvinyl alcohol: synthesis,

characterization, and degradation studies of the methyl orange dye from synthetic wastewater. Polymers 13:1–13. https://doi.org/10.3390/polym13223911

99. Sathyanarayanan P, Raina G (2011) Coating thickness study of biopolymer-magnetite core–shell nanoparticles. Int J Nanosci 08:359–366. https://doi.org/10.1142/s0219581x09006274

100. Ma HL, Qi XR, Maitani Y, Nagai T (2007) Preparation and characterization of superparamagnetic iron oxide nanoparticles stabilized by alginate. Int J Pharm 333:177–186. https://doi.org/10.1016/j.ijpharm.2006.10.006

101. Zhang PB, Liu P, Fan MM, Jiang PP, Haryono A (2021) High-performance magnetite nanoparticles catalyst for biodiesel production: Immobilization of 12-tungstophosphoric acid on SBA-15 works effectively. Renew Energ 175:244–252. https://doi.org/10.1016/j.renene.2021.05.033

102. Sima F, Ristoscu C, Duta L, Gallet O, Anselme K, Mihailescu IN (2016) Laser thin films deposition and characterization for biomedical applications. In: Laser surface modification of biomaterials. Woodhead Publishing, pp 77–125

103. Pantilimon MC, Dragan CI, Gradinaru C, Predescu AM, Sohaciu M, Coman G, Matei E, Predescu C (2018) Morphological analysis of magnetic nanomaterials through comparative methods. Univ Politeh Buchar 80:175–182

104. Ingham B, Toney MF (2014) X-ray diffraction for characterizing metallic films. In: Metallic films for electronic, optical and magnetic applications. Woodhead Publishing pp 3–38

105. Narayanaswamy V, Sambasivam S, Saj A, Alaabed S, Issa B, Al-Omari IA, Obaidat IM (2021) Role of magnetite nanoparticles size and concentration on hyperthermia under various field frequencies and strengths. Molecules 26:1–14. https://doi.org/10.3390/molecules26040796

106. Shi D, Sadat ME, Dunn AW, Mast DB (2015) Photo-fluorescent and magnetic properties of iron oxide nanoparticles for biomedical applications. Nanoscale 7:8209–8232. https://doi.org/10.1039/c5nr01538c

107. Predescu AM, Vidu R, Predescu A, Matei E, Pantilimon C, Predescu C (2019) Synthesis and characterization of bimodal structured Cu-Fe_3O_4 nanocomposites. Powder Technol 342:938–953. https://doi.org/10.1016/j.powtec.2018.10.015

108. Usman M, Byrne JM, Chaudhary A, Orsetti S, Hanna K, Ruby C, Kappler A, Haderlein SB (2018) Magnetite and green rust: synthesis, properties, and environmental applications of mixed-valent iron minerals. Chem Rev 118:3251–3304. https://doi.org/10.1021/acs.chemrev.7b00224

109. Kim W, Suh CY, Cho SW, Roh KM, Kwon H, Song K, Shon IJ (2012) A new method for the identification and quantification of magnetite-maghemite mixture using conventional X-ray diffraction technique. Talanta 94:348–352. https://doi.org/10.1016/j.talanta.2012.03.001

110. Azcona P, Zysler R, Lassalle V (2016) Simple and novel strategies to achieve shape and size control of magnetite nanoparticles intended for biomedical applications. Colloid Surf A 504:320–330. https://doi.org/10.1016/j.colsurfa.2016.05.064

111. Che Soh S, mohd yusof M, Abd Rahman Azmi A, Shamsuddin M, Wan Nor WF. (2018) Synthesis and physicochemical properties of magnetite nanoparticles (Fe_3O_4) as potential solid support for homogeneous catalysts. Malaysian J Anal Sci 22:768–774. https://doi.org/10.17576/mjas-2018-2205-04

112. Liang Y, Lu WL (2020) Gamma-irradiation synthesis of Fe_3O_4/rGO nanocomposites as lithium-ion battery anodes. J Mater Sci 31:17075–17083. https://doi.org/10.1007/s10854-020-04268-9

113. Sun XH, Zheng CM, Zhang FX, Yang YL, Wu GJ, Yu AM, Guan NJ (2009) Size-controlled synthesis of magnetite (Fe_3O_4) nanoparticles coated with glucose and gluconic acid from a single Fe(III) precursor by a sucrose bifunctional hydrothermal method. J Phys Chem C 113:16002–16008. https://doi.org/10.1021/jp9038682

114. Chang Y, Bai YP, Teng B, Li ZL (2009) A new drug carrier: magnetite nanoparticles coated with amphiphilic block copolymer. Chinese Sci Bull 54:1190–1196. https://doi.org/10.1007/s11434-009-0144-0

115. Ziegler-Borowska M, Chelminiak D, Kaczmarek H (2015) Thermal stability of magnetic nanoparticles coated by blends of modified chitosan and poly(quaternary ammonium) salt. J Therm Anal Calorim 119:499–506. https://doi.org/10.1007/s10973-014-4122-7

116. Lesiak B, Rangam N, Jiricek P, Gordeev I, Toth J, Kover L, Mohai M, Borowicz P (2019) Surface study of Fe_3O_4 nanoparticles functionalized with biocompatible adsorbed molecules. Front Chem 7:642. https://doi.org/10.3389/fchem.2019.00642

117. Babick F (2020) Dynamic light scattering (DLS). In: Characterization of nanoparticles. Elsevier: pp 137–172

118. ISO 22412:2017(E) (2017) Particle size analysis—dynamic light scattering (DLS). In: International Organization for Standardization
119. Lim J, Yeap SP, Che HX, Low SC (2013) Characterization of magnetic nanoparticle by dynamic light scattering. Nanoscale Res Lett 8:381. https://doi.org/10.1186/1556-276X-8-381
120. Arévalo-Cid P, Isasi J, Caballero AC, Martín-Hernández F, González-Rubio R (2022) Effects of shell-thickness on the powder morphology, magnetic behavior and stability of the chitosan-coated Fe3O4 nanoparticles. Bol Soc Esp Ceram Vidr 61:300–312. https://doi.org/10.1016/j.bsecv.2020.12.001
121. Brookhaven CI (2019) Using dynamic light scattering (DLS) to detect the onset of aggregation as a function of ph of iron oxide nanopowder. In: AZO Materials. https://www.azom.com/article.aspx?ArticleID=18154
122. Xu Y, Qin Y, Palchoudhury S, Bao Y (2011) Water-soluble iron oxide nanoparticles with high stability and selective surface functionality. Langmuir 27:8990–8997. https://doi.org/10.1021/la201652h
123. Gonzales M, Krishnan KM (2007) Phase transfer of highly monodisperse iron oxide nanocrystals with Pluronic F127 for biomedical applications. J Magn Magn Mater 311:59–62. https://doi.org/10.1016/j.jmmm.2006.10.1150
124. Baer DR (2020) Guide to making XPS measurements on nanoparticles. J Vac Sci Technol A 38:031201. https://doi.org/10.1116/1.5141419
125. Glaria A, Soule S, Hallali N, Ojo WS, Mirjolet M, Fuks G, Cornejo A, Allouche J, Dupin JC, Martinez H, Carrey J, Chaudret B, Delpech F, Lachaize S, Nayral C (2018) Silica coated iron nanoparticles: synthesis, interface control, magnetic and hyperthermia properties. RSC Adv 8:32146–32156. https://doi.org/10.1039/c8ra06075d
126. Grosvenor AP, Kobe BA, Biesinger MC, McIntyre NS (2004) Investigation of multiplet splitting of Fe 2p XPS spectra and bonding in iron compounds. Surf Interface Anal 36:1564–1574. https://doi.org/10.1002/sia.1984
127. Biesinger MC, Payne BP, Grosvenor AP, Lau LWM, Gerson AR, Smart RS (2011) Resolving surface chemical states in XPS analysis of first row transition metals, oxides and hydroxides: Cr, Mn, Fe, Co and Ni. Appl Surf Sci 257:2717–2730. https://doi.org/10.1016/j.apsusc.2010.10.051
128. Zhang S, Li XY, Chen JP (2010) An XPS study for mechanisms of arsenate adsorption onto a magnetite-doped activated carbon fiber. J Colloid Interface Sci 343:232–238. https://doi.org/10.1016/j.jcis.2009.11.001
129. Yau XH, Yew KY, Khe CS, Rajalingam S, Lai CW, Liu WW (2017) Facile one pot synthesis of highly stable L-ascorbic acid coated magnetite nanoparticles dispersion. Dig J Nanomater Bios 12:401–413
130. Powell CJ, Werner WSM, Kalbe H, Shard AG, Castner DG (2018) Comparisons of analytical approaches for determining shell thicknesses of core-shell nanoparticles by X-ray photoelectron spectroscopy. J Phys Chem 122:4073–4082. https://doi.org/10.1021/acs.jpcc.7b12070
131. Baer DR, Wang YC, Castner DG (2016) Use of XPS to quantify thickness of coatings on nanoparticles. Micros Today 24:40–45. https://doi.org/10.1017/S1551929516000109
132. ISO 19749:2021 (2021) Nanotechnologies—Measurements of particle size and shape distributions by scanning electron microscopy. In: International organization for standardization
133. Xu WX, Geissman JW, VanderVoo R, Peacor DR (1997) Electron microscopy of iron oxides and implications for the origin of magnetizations and rock magnetic properties of Banded Series rocks of the Stillwater Complex, Montana. J Geophys Res-Sol Ea 102:12139–12157. https://doi.org/10.1029/97jb00303
134. Konopka J (2013) Quantitative differentiation of three iron oxides by EDS. Microsc Microanal 19:1046–1047. https://doi.org/10.1017/s1431927613007228
135. Grant DC, Goudie DJ, Voisey C, Shaffer M, Sylvester P (2018) Discriminating hematite and magnetite via scanning electron microscope-mineral liberation analyzer in the -200 mesh size fraction of iron ores. Appl Earth Sci 127:30–37. https://doi.org/10.1080/03717453.2017.1422334
136. Temelie M, Popescu RC, Cocioaba D, Vasile B, Savu D (2018) Biocompatibility study of magnetite nanoparticle synthesized using a green method. Rom J Phys 63:1–13
137. Ardelean IL, Stoencea LBN, Ficai D, Ficai A, Trusca R, Vasile BS, Nechifor G, Andronescu E (2017) Development of stabilized magnetite nanoparticles for medical applications. J Nanomater 2017:6514659. https://doi.org/10.1155/2017/6514659
138. ISO 21363:2020 (2020) Nanotechnologies—Measurements of particle size and shape distributions by transmission electron microscopy. In: International Organization for Standardization

139. Deng YH, Wang CC, Hu JH, Yang WL, Fu SK (2005) Investigation of formation of silica-coated magnetite nanoparticles via sol-gel approach. Colloid Surf A 262:87–93. https://doi.org/10.1016/j.colsurfa.2005.04.009

140. Gupta J, Hassan PA, Barick KC (2021) Core-shell Fe_3O_4@ZnO nanoparticles for magnetic hyperthermia and bio-imaging applications. AIP Adv 11:025207. https://doi.org/10.1063/9.0000135

141. Faaliyan K, Abdoos H, Borhani E, Afghahi SSS (2018) Magnetite-silica nanoparticles with core-shell structure: single-step synthesis, characterization and magnetic behavior. J Sol-Gel Sci Technol 88:609–617. https://doi.org/10.1007/s10971-018-4847-z

142. Deng Y, Qi D, Deng C, Zhang X, Zhao D (2008) Superparamagnetic high-magnetization microspheres with an Fe_3O_4@SiO_2 core and perpendicularly aligned mesoporous SiO_2 shell for removal of microcystins. J Am Chem Soc 130:28–29. https://doi.org/10.1021/ja0777584

143. Avval ZM, Malekpour L, Raeisi F, Babapoor A, Mousavi SM, Hashemi SA, Salari M (2020) Introduction of magnetic and supermagnetic nanoparticles in new approach of targeting drug delivery and cancer therapy application. Drug Metab Rev 52:157–184. https://doi.org/10.1080/03602532.2019.1697282

144. Bhattacharya S (2021) Nanostructures in gene delivery. In: Bajpai AK, Saini RK (eds) Advances in polymeric nanomaterials for biomedical applications. Elsevier, Amsterdam, pp 101–135

145. Ganapathe LS, Mohamed MA, Yunus RM, Berhanuddin DD (2020) Magnetite (Fe3O4) nanoparticles in biomedical application: From synthesis to surface functionalisation. Magnetochemistry 6:68. https://doi.org/10.3390/magnetochemistry6040068

146. Maity D, Kale SN, Kaul-Ghanekar R, Xue JM, Ding J (2009) Studies of magnetite nanoparticles synthesized by thermal decomposition of iron (III) acetylacetonate in tri(ethylene glycol). J Magn Magn Mater 321:3093–3098. https://doi.org/10.1016/j.jmmm.2009.05.020

147. Zhang L, He R, Gu HC (2006) Oleic acid coating on the monodisperse magnetite nanoparticles. Appl Surf Sci 253:2611–2617. https://doi.org/10.1016/j.apsusc.2006.05.023

148. Zhou L, Ye L, Lu Y (2022) Flexible and effective preparation of magnetic nanoclusters via one-step flow synthesis. Nanomaterials. https://doi.org/10.3390/nano12030350

149. Circu M, Nan A, Borodi G, Liebscher J, Turcu R (2016) Refinement of magnetite nanoparticles by coating with organic stabilizers. Nanomater 6:1–12. https://doi.org/10.3390/nano6120228

150. Epp J (2016) X-ray diffraction (XRD) techniques for materials characterization. In: Materials characterization using nondestructive evaluation (NDE) methods. Woodhead Publishing, pp 81–124.

151. Mahdavi M, Ahmad MB, Haron MJ, Namvar F, Nadi B, Rahman MZ, Amin J (2013) Synthesis, surface modification and characterisation of biocompatible magnetic iron oxide nanoparticles for biomedical applications. Molecules 18:7533–7548. https://doi.org/10.3390/molecules18077533

152. Wang BY, Wei QF, Qu SL (2013) Synthesis and characterization of uniform and crystalline magnetite nanoparticles via oxidation-precipitation and modified co-precipitation methods. Int J Electrochem Sci 8:3786–3793. https://doi.org/10.1016/S1452-3981(23)14431-2

153. Tajabadi M, Khosroshahi M (2012) New finding on magnetite particle size reduction by changing temperature and alkaline media concentration. APCBEE Proc 3:140–146. https://doi.org/10.1016/j.apcbee.2012.06.060

154. Babes L, Denizot B, Tanguy G, Le Jeune JJ, Jallet P (1999) Synthesis of iron oxide nanoparticles used as MRI contrast agents: a parametric study. J Colloid Interface Sci 212:474–482. https://doi.org/10.1006/jcis.1998.6053

155. Nejabat S, Siadat SOR, Tahmasian Z, Mirzajani F, Fatemi F, Hosseinkhani S, Abedi MR (2021) How co-precipitation reaction parameters control the characteristics and features of iron oxide nanoparticles. Phys Chem Res 9:241–252. https://doi.org/10.22036/pcr.2020.251463.1843

156. Alibeigi S, Vaezi MR (2008) Phase transformation of iron oxide nanoparticles by varying the molar ratio of Fe^{2+}:Fe^{3+}. Chem Eng Technol 31:1591–1596. https://doi.org/10.1002/ceat.200800093

157. Khan US, Khattak NS, Rahman A, Khan F (2011) Optimal method for preparation of magnetite nanoparticles. J Chem Soc Pakistan 33:628–633

158. Ishii M, Nakahira M, Yamanaka T (1972) Infrared absorption spectra and cation distributions in $(Mn, Fe)_3O_4$. Solid State Commun 11:209–212. https://doi.org/10.1016/0038-1098(72)91162-3

159. Cui HT, Ren WZ, Lin P, Liu Y (2013) Structure control synthesis of iron oxide polymorph nanoparticles through an epoxide precipitation route. J Exp Nanosci 8:869–875. https://doi.org/10.1080/17458080.2011.616541

160. Roonasi P, Holmgren A (2009) A study on the mechanism of magnetite formation based on iron isotope fractionation. Epd Cong 25:829–836

161. Ercuta A, Chirita M (2013) Highly crystalline porous magnetite and vacancy-ordered maghemite microcrystals of rhombohedral habit. J Cryst Growth 380:182–186. https://doi.org/10.1016/j.jcrysgro.2013.06.003

162. Nasrazadani S (1997) The application of infrared spectroscopy to a study of phosphoric and tannic acids interactions with magnetite (Fe3O4), goethite (α-FEOOH) and lepidocrocite (γ-FeOOH). Corros Sci 39:1845–1859. https://doi.org/10.1016/s0010-938x(97)00060-7

163. Li YS, Church JS, Woodhead AL (2012) Infrared and Raman spectroscopic studies on iron oxide magnetic nano-particles and their surface modifications. J Magn Magn Mater 324:1543–1550. https://doi.org/10.1016/j.jmmm.2011.11.065

164. Žic M, Ristić M, Musić S (2011) Monitoring the hydrothermal precipitation of α-Fe2O3 from concentrated Fe(NO3)3 solutions partially neutralized with NaOH. J Mol Struct 993:115–119. https://doi.org/10.1016/j.molstruc.2010.09.048

165. Nangah CR, Merlain TG, Nsami NJ, Tubwoh CP, Foba-Tendo J, Mbadcam KJ (2019) Synthesized goethite and natural iron oxide as effective absorbents for simultaneous removal of Co(II) and Ni(II) ions from water. J Encapsulation Adsorpt Sci 09:127–147. https://doi.org/10.4236/jeas.2019.93007

166. Veneranda M, Aramendia J, Bellot-Gurlet L, Colomban P, Castro K, Madariaga JM (2018) FTIR spectroscopic semi-quantification of iron phases: A new method to evaluate the protection ability index (PAI) of archaeological artefacts corrosion systems. Corros Sci 133:68–77. https://doi.org/10.1016/j.corsci.2018.01.016

167. López J, González F, Bonilla F, Zambrano G, Gomez M (2010) Synthesis and characterization of Fe3O4 magnetic nanofluid. Rev LatinAm Metal 30:60–66

168. Bordbar AK, Rastegari AA, Amiri R, Ranjbakhsh E, Abbasi M, Khosropour AR (2014) Characterization of modified magnetite nanoparticles for albumin immobilization. Biotechnol Res Int 2014:705068. https://doi.org/10.1155/2014/705068

169. Zheng L, Su W, Qi Z, Xu Y, Zhou M, Xie Y (2011) First-order metal-insulator transition and infrared identification of shape-controlled magnetite nanocrystals. Nanotechnol 22:485706. https://doi.org/10.1088/0957-4484/22/48/485706

170. Sarma L, Borah JP, Srinivasan A, Sarma S (2020) Synthesis and characterization of tea polyphenol-coated magnetite nanoparticles for hyperthermia application. J Supercond Nov Magn 33:1637–1644. https://doi.org/10.1007/s10948-019-05189-3

171. Maleki A, Azizi M, Emdadi Z (2018) A novel poly(ethyleneoxide)-based magnetic nanocomposite catalyst for highly efficient multicomponent synthesis of pyran derivatives. Green Chem Lett Rev 11:573–582. https://doi.org/10.1080/17518253.2018.1547795

172. Jin XD, Zhang KY, Sun J, Wang J, Dong ZP, Li R (2012) Magnetite nanoparticles immobilized Salen Pd (II) as a green catalyst for Suzuki reaction. Catal Commun 26:199–203. https://doi.org/10.1016/j.catcom.2012.05.026

173. Kazemzadeh H, Ataie A, Rashchi F (2012) Synthesis of magnetite nano-particles by reverse co-precipitation. Int J Mod Phys: Conf 05:160–167. https://doi.org/10.1142/s2010194512001973

174. Xie WL, Xiong YF, Wang HY (2021) Fe3O4-poly(AGE-DVB-GMA) composites immobilized with guanidine as a magnetically recyclable catalyst for enhanced biodiesel production. Renew Energ 174:758–768. https://doi.org/10.1016/j.renene.2021.04.086

175. Dheyab MA, Aziz AA, Jameel MS, Noqta OA, Khaniabadi PM, Mehrdel B (2020) Simple rapid stabilization method through citric acid modification for magnetite nanoparticles. Sci Rep 10:10793. https://doi.org/10.1038/s41598-020-67869-8

176. Fan GY, Ren YL, Jiang WD, Wang CY, Xu B, Liu F (2014) Effective catalytic hydrodechlorination of 4-chlorophenol over a Rh immobilized on amine-functionalized magnetite nanoparticles in aqueous phase. Catal Commun 52:22–25. https://doi.org/10.1016/j.catcom.2014.04.006

Authors and Affiliations

Ancuţa Roxana Trifoi[2] · Ecaterina Matei[2] · Maria Râpă[2] · Andrei-Constantin Berbecaru[2] · Caşen Panaitescu[1] · Ionut Banu[3] · Rami Doukeh[1]

✉ Rami Doukeh
rami.doukeh@yahoo.com; rami.doukeh@upg-ploiesti.ro

Ancuţa Roxana Trifoi
ancuta_trifoi@yahoo.com

Ecaterina Matei
ecaterina.matei@upb.ro

Maria Râpă
maria.rapa@upb.ro

Andrei-Constantin Berbecaru
andrei.berbecaru@upb.ro

Caşen Panaitescu
cpanaitescu@upg-ploiesti.ro

Ionut Banu
i_banu@chim.upb.ro

[1] Faculty of Material Science and Engineering, University POLITEHNICA of Bucharest, 313 Splaiul Independenţei, 060042 Bucharest, Romania

[2] Chemical and Biochemical Engineering Department, University POLITEHNICA of Bucharest, 1-7 Polizu Str., RO, 011061 Bucharest, Romania

[3] Faculty of Petroleum and Gas Engineering, Faculty of Petroleum Refining and Petrochemistry, Petroleum-Gas University of Ploieşti, 39 Bucharest Blvd., 100680 Ploieşti, Romania